BBA - Molecular Basis of Disease 1864 (2018) 1754–1769

Contents lists available at ScienceDirect

BBA - Molecular Basis of Disease

journal homepage: www.elsevier.com/locate/bbadis

PD-L1 confers glioblastoma multiforme malignancy via Ras binding and Ras/Erk/EMT activation

Xin Yao Qiu[a,1], Dian Xing Hu[a,1], Wen-Qiang Chen[b], Ruo Qiao Chen[c], Shi Rui Qian[c], Chun Yang Li[a], Yuan Jun Li[a], Xin Xin Xiong[a], Di Liu[d], Feng Pan[d], Shang Bin Yu[a], Xiao Qian Chen[a,*]

[a] Department of Pathophysiology, School of Basic Medicine, Tongji Medical College, Institute of Brain Research, Key Laboratory of Neurological Diseases, Ministry of Education, Hubei Provincial Key Laboratory of Neurological Diseases, Huazhong University of Science and Technology, Wuhan 430030, China
[b] Program in Cellular and Molecular Medicine, Boston Children's Hospital, Harvard Medical School, 200 Longwood Avenue, Boston, MA 02115, USA
[c] School of Basic Medicine, Tongji Medical College, Huazhong University of Science and Technology, Wuhan 430030, China
[d] Department of Urology, Union Hospital, Tongji Medical College, Huazhong University of Science and Technology, Wuhan 430022, China

ARTICLE INFO

Keywords:
B7-H1
Vimentin
Bioluminescence imaging
Protein-protein interaction
Brain tumor

ABSTRACT

Glioblastoma multiforme (GBM) is the most aggressive primary brain tumor due to the lack of effective therapeutic drugs. Cancer therapy targeting programmed cell death protein 1 (PD-1) or programmed death ligand-1 (PD-L1) is of revolutionary. However, the role of intrinsic PD-L1, which determines immune-therapy outcomes, remains largely unclear. Here we demonstrated an oncogenic role of PD-L1 via binding and activating Ras in GBM cells. RNA-sequencing transcriptome data revealed that PD-L1 significantly altered gene expression enriched in cell growth/migration/invasion pathways in human GBM cells. PD-L1 overexpression and knockout or knockdown demonstrated that PD-L1 promoted GBM cell proliferation and migration in vitro and in vivo. Mechanistically, PD-L1 prominently activated epithelial mesenchymal transition (EMT) process in a MEK/Erk- but not PI3K/Akt-dependent manner. Further, we identified intracellular interactions of PD-L1 and H-Ras, which led to Ras/Erk/EMT activation. Finally, we demonstrated that PD-L1 overexpression promoted while knockdown abolished GBM development and invasion in orthotopic GBM models of rodents. Taken together, we found that intracellular PD-L1 confers GBM cell malignancy and aggressiveness via binding Ras and activating the downstream Erk-EMT signaling. Thus, these results shed important insights in improving efficacy of immune therapy for GBM as well as other malignant tumors.

1. Introduction

Glioblastoma multiforme (GBM) is the most severe malignant astrocytoma (WHO grade IV), accounting for approximately 60%–70% of gliomas [1]. GBM is characterized by infiltrative growth, necrosis and hypoxia, with a median survival time of 14.6 months after diagnosis [2]. Despite the use of standard treatment regimen (i.e., surgical resection, radiotherapy and chemotherapy), the overall 5-year survival rate of GBM remains only 9.8% [2–4]. Therefore, identification of new therapeutic targets is urgent for improving GBM management.

Recently, antibodies against programmed cell death protein 1 (PD-1) and its ligand programmed death ligand-1 (PD-L1, i.e., CD274 or B7-H1) have been achieved curable results in advanced cancers (e.g., melanoma) and this antibody-based immune therapy is widely tested in different types of malignant tumors [5]. PD-1 exists mainly on cell surface of cytotoxic T lymphocytes (CTL) while PD-L1 is widely expressed in tumor and non-tumor cells (e.g., dendritic cells and monocytes) [5,6]. The binding of PD-L1 to PD-1 induces apoptosis or

Abbreviations: BLI, bioluminescence imaging; BSA, bovine serum albumin; CTL, cytotoxic T lymphocytes; CRISPR/Cas, Clustered Regularly Interspaced Short Palindromic Repeats/CRISPR associated nucleases; DEGs, differently expressed genes; DMEM, Dulbecco's modified Eagle's medium; EdU, 5-ethynyl-2-deoxyuridine; EGFP, enhanced green fluorescent protein; EMT, epithelial mesenchymal transition; FBS, Fetal Bovine Serum; GST, glutathione S-transferase; GBM, glioblastoma multiforme; GFP, green fluorescent protein; GO, Gene Ontology; GSK3, glycogen synthase kinase 3; H&E, hematoxylin-eosin; HIF, hypoxia-inducible factor; IHC, immunohistochemistry; IPP, Image-Pro Plus; KEGG, Kyoto Encyclopedia of Genes and Genomes; LV, lentivirus; MAPK, mitogen-activated protein kinase; MTT, 3-(4, 5-dimethylthiazol-2-yl)-2,5-diphenyltetrazolium bromide; PBS, phosphate buffer saline; PD-1, programmed cell death protein 1; PD-L1, programmed death ligand-1; PFA, paraformaldehyde; PI3K, phosphatidylinositol-4,5-bisphosphate 3-kinase; RBD, Ras-binding domain; shRNA, short hairpin RNA; sgRNA, single guide RNA; SD, Sprague-Dawley

* Corresponding author at: Hangkong Road 13, Wuhan 430030, China.
E-mail address: chenxq@mails.tjmu.edu.cn (X.Q. Chen).
[1] These authors contributed equally to the work.

https://doi.org/10.1016/j.bbadis.2018.03.002
Received 20 December 2017; Received in revised form 8 February 2018; Accepted 1 March 2018
Available online 03 March 2018

exhaustion of CTL, which constitutes the immune-inhibitory checkpoint responsible for escape of cancer cells from CTL's killing [5,6]. Present clinical data reveal that only a few patients respond positively to the therapy of PD-1/PD-L1 antibody, which largely depends on the immune status of the patients and the expression levels and functionality of PD-L1 in cancer cells [7–9]. The majority of the previous PD-L1 studies have been focused on analyzing the prognostic value of PD-L1 expression, demonstrating that PD-L1 is a key poor prognostic marker in various cancers, for example, breast cancer, renal cell carcinoma, melanoma and ovarian cancer [10–14]. Further, the regulation of PD-L1 expression is well studied, and it was reported that PD-L1 is upregulated by PI3K/PTEN/Akt, Erk, JAK/STAT3, hypoxia-inducible factors (HIF), nuclear factor kappa B and some other intracellular signaling pathways [15,16].

PD-L1 not only mediates tumor-CTL communications, but also exerts independent intracellular functions in cancer cells. Recently, it becomes aware that intrinsic PD-L1 plays important regulatory roles in cell growth, proliferation, apoptosis, autophagy, migration and invasion in various cancers, including melanoma [17], gastric cancer [18], pancreatic cancer [19], head and neck carcinoma [20], lung adenocarcinoma [21], suggesting that it might exert initial oncogenic effects in cancer development [22]. In ovarian cancer and melanoma cells, PI3K/Akt is strongly involved in PD-L1 oncogenic effects [17]. However, the underlying mechanism of intrinsic PD-L1 in most cancer cells remains largely unexplored.

Until now, clinical trials of PD-1 and PD-L1 antibodies in glioma remains in phase II and phase III, such as (1) NCT02017717, Nivolumab in GBM, was in phase III, and (2) NCT01952769, Pidilizumab in diffuse intrinsic pontine glioma, was in phase I and II [9]. Several studies had reported that higher PD-L1 expression level positively correlates to higher malignant grade of gliomas and poorer prognosis [23–27], and higher vascular endothelial growth factor level [28], supporting the oncogenic role of PD-L1 in glioma. In glioma tissues, increased PD-L1 appears mainly in Ki67-negative tumor cells, indicating that the major function of PD-L1 in glioma cells is not associated with cell proliferation [24]. Surprisingly, to our best knowledge, experimental study of intrinsic PD-L1 in glioma cells has not been reported.

In the present study, we demonstrated that intrinsic PD-L1 had prominent oncogenic effects, preferentially in aspects of promoting migration and invasion, on GBM cells in vitro and in vivo. We identified the first intracellular PD-L1-binding partner, Ras. Further, we demonstrated that PD-L1 enhanced GBM malignancy via activating Ras-Erk-EMT (epithelial mesenchymal transition) axis signaling.

2. Materials and methods

2.1. Cell culture, antibodies and pharmacological drugs

The human glioblastoma cell lines (U87MG, LN229), rat glioma C6 cell line, human embryonic kidney 293 T cell line were purchased from American Tissue Culture Collection (MA, USA). The human GBM cell line U251 was purchased from China Center for Type Culture Collection (Wuhan, China). All GMB cell lines were cultured in Dulbecco's modified Eagle's medium (DMEM, Gibco, CA, USA) supplemented with 10% FBS (Gemini, CA, USA) and 1% Penicillin-Streptomycin Solution (Hyclone, Thermo, Beijing, China). U0126 (MEK1/2 inhibitor, Cell Signaling Technology, MA, USA), LY294002 (PI3 kinase inhibitor, Cell Signaling Technology, MA, USA) or SB415286 (GSK3 inhibitor, Sigma, MO, USA) were used at a final concentration of 20 μM, 25 μM, or 20 μM, respectively. SCH772984 (specific Erk1/2 inhibitor, Sellcek Chemicals, Shanghai, China) were used at a final concentration of 0.5 or 1.0 μM. Primary antibodies against Slug (C15D3), β-catenin (D10A8), ZEB1 (D80D3), vimentin (D21H3), *E*-Cadherin (24E10), N-Cadherin (D4R1H), phospho-p44/42 MAP kinase (Thr202/Tyr204, #9101), p44/42 MAPK (137F5), phospho-Akt (Ser473, #D9E), total Akt (#9272), GSK-3β (27C10), phospho-GSK-3β (Ser9, #9336) were purchased from Cell Signaling Technology (MA, USA). Antibodies against PD-L1/CD274 (PA5-28115, Thermo Fisher, IL, USA), PD-L1 (ABM4E54, Abcam, Cambridge, UK), GST (Z-5, Santa Cruz Biotechnology, TX, USA), β-actin (20536–1-AP, Proteintech, Wuhan, China) were commercially purchased.

2.2. Establishment of stable GBM cell lines with PD-L1 overexpression

p-PD-L1-EGFP-GV230 plasmid expressing PD-L1-EGFP fusion protein was purchased from GeneChem (Shanghai, China). Full-length human PD-L1 coding cDNA with stop codons was PCR amplified from p-PD-L1-EGFP-GV230 plasmids and cloned into lentiviral p-FU vector (p-FU-PD-L1). Lentivirus/p-FU-PD-L1 (LV-PD-L1), Lentivirus/p-FU (LV-Vec) or Lentivirus/p-FU-Venus (LV-Venus) were packaged in 293 T cells, purified and concentrated using Amicon Ultra-15 Centrifugal Filters (Ultracel-100 K, Merck Millipore Ltd., Cork, Ireland), and then aliquoted and stored at −80 °C. Concentrated LV solution at a final concentration of 1/50 were used for lentiviral infection of U251/U87MG/LN229/C6 cells (efficiency > 90% as determined by Venus expression, Fig. S1) and the expression of exogenous gene remained unchanged after at least 10 passages.

2.3. Establishment of stable GBM cell lines with PD-L1 knockdown

Lentivirus containing human PD-L1 short hairpin RNA (shRNA) targeting 5′-CGAATTACTGTGAAAGTCAAT-3′ (LV-sh-PD-L1) and control LV-sh-NC (1×10^8 TU/ml, with EGFP tag) was purchased from Vigene (Shandong, China). Condensed LV-sh-PD-L1 or LV-sh-NC at a final concentration of 1/500 was used for viral infection of U251/U87MG cells.

2.4. Establishment of stable GBM cell lines with PD-L1 knockout via CRISPR/Cas9 technique

CRISPR/Cas9 technique utilizes a single guide RNA (sgRNA) scaffold to direct genomic DNA cutting by Cas9, which leads to reading-frame shift of the cutting gene after repairing and thus abolishes normal functions of the gene/protein [29,30]. DNA oligos encoding specific sgRNA targeting to human PD-L1 genome or GFP (served as control) were selected from genome-scale CRISPR knock-out (GeCKO) libraries [29,30]:

CRISPR GFP#1 Forward: CACCGGGAGCGCACCATCTTCTTCA.
CRISPR GFP#1 Reverse: AAACTGAAGAAGATGGTGCGCTCCC.
CRISPR PD-L1#2 Forward: CACCGAGCTACTATGCTGAACCTTC.
CRISPR PD-L1#2 Reverse: AAACGAAGGTTCAGCATAGTAGCTC.
CRISPR PD-L1#3 Forward: CACCGGGATGACCAATTCAGCTGTA.
CRISPR PD-L1#3 Reverse: AAACTACAGCTGAATTGGTCATCCC.

The oligo DNA pairs were commercially synthesized, annealed and inserted into LentiCRISPRv2 (Invitrogen, CA, USA) at *Bsm*BI/BsmBI sites (named LV-sg-GFP/sg-PD-L1#2/sg-PD-L1#3), which expresses specific sgRNAs and Cas9 protein. Lentiviruses were produced, purified and concentrated as LV-Venus. Condensed LV-sg-GFP/sg-PD-L1#2/sg-PD-L1#3 at a final concentration of 1/50 was used to infect U251/U87MG cells. Puromycin at a final concentration of 2.0 μg/ml (Selleck Chemicals, TX, USA) was used to select stable sgRNA/Cas9-expressing cells. U87MG/sg-PD-L1 cells were collected as a pool while U251/sg-PD-L1 cells were multiplied from a single clone.

2.5. Orthotopic rat/mouse models of GBM and bioluminescence imaging

All animal handling and experiments were performed in accordance with NIH guidelines and approved by the Ethics Committees of Huazhong University of Science and Technology. Adult Sprague-Dawley (SD) rats (250–300 g, male) were purchased from the Experimental Animal Centre, HUST and Balb/c nude mice (4–5 weeks old, body weight 16–18 g, female) were purchased from Beijing Vital

River Laboratory Animal Technology Company (Beijing, China). All animals were group housed in the Animal Core Facility of Tongji Medical College with a 12-h light/dark cycle with ad libitum to food and water for 3 days prior to any experiments. GBM cell implantation in the brain was performed as previously described [31]. Briefly, adult rats were anesthetized with chloral hydrate and a burr hole was drilled in the skull 1.0 mm anterior to the bregma and 3.2 mm left or right to the sagittal suture. A 10-μl Hamilton microsyringe (Hamilton, MA, USA) with an unbeveled 33G needle containing 1.0×10^6 of C6/Vec (left) or C6/PD-L1 (right) cells in 10 μl of PBS was advanced to a depth of 5.3 mm from the skull surface and then withdrawed 0.5 mm. Cell suspension was delivered at rate of 1.0 μl/min. After cell implantation, the needle was left in place for 10 min before withdrawal. After 14 d of cell inoculation, the rats were perfused with 4% paraformaldehyde (PFA) and the brains were paraffin-embedded. For nude mouse GBM model, equal amounts of U87MG cells (2.5×10^5 cells in 3 μl of PBS) with LV-sh-NC or sh-PD-L1 infection (with EGFP tag) were implanted into the left (U87MG/sh-NC) or right (U87MG/sh-PD-L1) striatum of brain at 0.5 mm anterior to the bregma/2.0 mm left or right to the sagittal suture/3.2 mm depth from the skull surface. After 24 d of cell inoculation, nude mice were anesthetized and imaged for EGFP activity at 488 nm-excitation using a bioluminescence imaging (BLI) system-Lago X (Spectral Instruments Imaging, AZ, USA). Immediately after living imaging, the mice were sacrificed and perfused with 4% PFA. The whole brains were isolated and rescanned for EGFP images. The BLI data was analyzed by Amiview (Spectral Instruments Imaging, AZ, USA) and expressed as average radiance ($\times 10^7$ photons/s/cm^2/sr) [32].

2.6. RNA-sequencing and enrichment analysis

Three 100-mm dishes of U251/PD-L1 or U251/Vec stable cell lines were subjected to total mRNA isolation, cDNA libraries construction and sequencing at Illumina HiSeq sequence platform (PE150) with 6G clean data by Novogene Bioinformatics Institute (Shanghai, China). Differential gene expression analysis between U251/PD-L1 and U251/Vec groups was performed using the DESeq2 R package (1.10.1). The resulting *P*-values were adjusted using the Benjamini and Hochberg's approach for controlling the false discovery rate. Differently expressed genes (DEGs) with $P < 0.005$, adjusted $P < 0.05$ (*P*adj) and absolute changing fold ≥ 1.2 were subjected to Kyoto Encyclopedia of Genes and Genomes (KEGG) pathway and Gene Ontology (GO) enrichment analysis. KEGG pathways and GO terms with *P*adj < 0.05 were considered significantly enriched by DEGs.

2.7. Cell viability and EdU-incorporation assays

The 3-(4, 5-dimethylthiazol-2-yl)-2,5-diphenyltetrazolium bromide (MTT) assay was used to measure cell viability as previously reported [33]. GBM cells were seeded in 96-well plates (3000 cells/well). MTT (1 mg/ml of final concentration; Amresco Inc., OH, USA) was added to each well at a fixed time every day, and 100 μl of dimethyl sulfoxide was added to each well 4 h after incubation. The optical density of solution was measured at absorbance 490/650 nm with a microtiter plate reader (Synergy 2, BioTek Instruments, VT, USA). The absorbance at 490 nm minus absorbance at 650 nm represented cell viability. Results were shown as the relative cell viability compared to 0 d with at least 6 replicates.

EdU (5-ethynyl-2-deoxyuridine)-incorporation assay was conducted as reported [33] using EdU DNA Proliferation in vitro Detection kit (RiboBio, Guangzhou, China). Briefly, GBM cells were seeded in 96-well plates (1×10^4 cells/well) in triplicate for 24 h, incubated with 50 μM of EdU for another 2 h and then the EdU incorporation was manifested by Apollo® fluorochrome according to the manufacturer's instructions. Nuclei were stained with Hoechst 33,342 in the kit. Micrographs were taken randomly from at least 9 different fields in each well with a conventional inverted fluorescent microscope (Olympus, Tokyo, Japan) and the percentage of EdU-positive cells was calculated as the number of EdU-positive cell divided by the number of Hoechst-positive cells.

2.8. Scratch-wound healing assay, cell morphology analysis and transwell-migration assay

Cell migration ability was measured by scratch-wound healing assay as previously reported [34]. Briefly, confluent cells in 35-mm dishes were scratched with a yellow pipette and the wound edges were micrographed at 0 h and designated time-points. The wound-edge line was drawn by linking front boundary of at least 10 cells forward the nude area. The wound size was calculated as the distance between the opposite wound-edge lines using the Image-Pro Plus (IPP) software (Media Cybernetics, USA) and the average wound size represented at least 12 different fields in each culture dish. Cell morphology analysis was conducted as reported [35]. For cell length/width and cell pseudopodia length measurement, single cells along the wound edge or in the nude area were randomly selected for analysis using the IPP software as supplemental instructions (Fig. S2). Data from at least 200 cells were used for statistical analysis.

Transwell-migration assay was conducted as reported [34]. Briefly, 1×10^5 cells were seeded into the upper chamber of transwell apparatus (Corning Incorporated, NY, USA) in 200 μl of serum-free DMEM and 800 μl of complete medium was added to the lower chamber to induce cell migration. After 12 h, migrated cells were stained, micrographed and calculated. An average of migrated cells from at least 9 different fields was used for statistical analysis.

2.9. Western blotting analysis

Western blotting analysis was performed as previously reported [36]. Briefly, the cell lysates were collected and dispersed in radioimmunoprecipitation assay lysis buffer containing phenylmethanesulfonyl fluoride. Equal amounts of total proteins were subjected to sodium dodecyl sulfate polyacrylamide gel electrophoresis and electrotransferred onto nitrocellulose filter membranes (0.45 μm, Merck Millipore, Cork, Ireland). The blots were incubated with corresponding primary and secondary IRDye 800 or IRDye 680 CW-conjugated goat anti-rabbit or anti-mouse IgG antibodies (LI-COR Biosciences, Lincoln, USA). The labeled bands were visualized and quantified by Odyssey Infrared Imaging System (LI-COR Biosciences, MA, USA).

2.10. Immunofluorescence staining and analysis

Immunofluorescence staining was performed as previously reported [36]. Cells in 35-mm culture dishes were fixed, permeabilized, blocked, and then incubated with primary and corresponding Dylight 488-labeled secondary antibodies (Abbkine, CA, USA). For paraffin-embedded tissues, rat brain slices were deparaffinized, rehydrated, antigen unmasked, blocked with 5% bovine serum albumin (BSA) and then incubated with primary antibodies and corresponding Dylight 488/594-labeled secondary antibodies. Micrographs were taken under the same conditions with a conventional fluorescent microscope (Olympus, Tokyo, Japan).

The clinical tumor sample was obtained from the Department of Pathology, Tongji Hospital, Huazhong University of Science and Technology. The sample was surgically resected during 2016 and diagnosed as GBM (WHO IV) clinically and pathologically at Tongji Hospital. Immunofluorescence staining was done with paraffin-embedded tissues as described above. Micrographs were taken with a Zeiss 510 confocal microscope (Carl Zeiss, Oberkochen, Germany). The fluorescence intensity of stained cells was analyzed with ImageJ (NIH, https://imagej.nih.gov/ij/).

2.11. Glutathione S-transferase (GST)-pull down assay

GST-pull down assay was performed as previously described [36]. LN229 or 293 T cells were transfected with pDEST27-GST/GST-H-Ras or co-transfected with p-FU-PD-L1 + pDEST27-GST/GST-H-Ras for 2 d. Cell lysates were extracted with GST-lysis buffer and 400 μg of total soluble proteins from each sample were incubated with 30 μl of glutathione sepharose bead slurry (GE Healthcare Life Sciences, Piscataway, USA) overnight at 4 °C. After extensive washing, the immunoprecipitates were subjected to Western blotting analysis. Anti-GST or anti-PD-L1 antibodies were used to probe corresponding proteins.

2.12. Active Ras detection assay

Active Ras detection assay was performed using Active Ras Dection Kit (#8821, Cell Signaling Technology, MA, USA) as manufacturer's instructions. GST-Raf1-RBD (Ras-binding domain) fusion protein is used to bind the activated form of Ras (GTP-bound Ras), which can then be immnunoprecipitated with glutathione resin. Briefly, cell lysate of U251/Vec or U251/PD-L1 cells of 100-mm dish was extracted with Lysis/Binding/Wash Buffer from the kit. Cell lysate (1 mg/ml) of 700 μg for each sample was subjected to a spin cup (inserted in collection tube) which was pretreated with 100 μl of 50% glutathione resin and 80 μg GST-Raf1-RBD, and then the mixture was incubated at 4 °C for 1 h with gentle rocking. In vitro GTPγS or GDP treatment with 700 μl equal mixed U251-Vec/PD-L1 cell lysate was set as positive or negative control respectively (not shown). A volume of 50 μl 2XSDS buffer (containing 200 mM dithiothreitol) was used to detach the reaction mixture from the spin cup. Heat the eluted samples for 5 min at 95–100 °C and then subjected to Western blotting analysis. Ras (GTP-bound Ras) level was detected using a Ras Mouse mAb from the kit.

2.13. Hematoxylin-eosin (H&E) staining and immunohistochemistry (IHC) analysis

Paraffin-embedded rat or mouse brain slices (4 μm) were used for H &E staining and the brain images were scanned with an automatic slice scanning system-SV120 (Olympus, Tokyo, Japan). The tumor rim was delineated with black dashed cycle. Tumor invasive index was calculated via measuring the area of tumor invading the brain parenchyma per tumor rim length as reported [31]. Statistical analysis used data from at least 7 slices from 5 rat brains per group. For IHC, the rat brain slices were deparaffinized, rehydrated, endogenous peroxidase blocked, antigen unmasked, blocked with 5% BSA and then incubated with primary antibodies and corresponding secondary antibodies. Immunoreaction was visualized with diamino-benzidine tetrachloride. The sections were photographed with an optical microscope (Olympus, Tokyo, Japan), and the integral optical density of positive signal was analyzed with ImageJ. Statistical analysis used data from at least 7 slices from 5 brains per group.

2.14. Statistical analysis

All experiments were repeated independently at least three times. The values were expressed as means ± SEM. Unpaired Student's test was used to compare between two groups of in vitro experiments. Paired Student's test was used to compare between two groups of animal experiments. Comparisons among multiple groups were performed through one-way ANOVA with Student–Newman–Keuls post-test. $P < 0.05$ was considered statistically significant.

3. Results

3.1. PD-L1 knockdown abolishes glioma xenografts formation in nude mice

We first studied the role of endogenous PD-L1 on GBM development using human GBM cells. Stable PD-L1 knockdown U87MG cell line (U87MG/sh-PD-L1 or negative control U87MG/sh-NC, both with EGFP tag) was established by lentivirus infection, which was confirmed by Western blotting analysis (Fig. 3G and Fig. S5A). Equal amounts of U87MG/sh-NC or U87MG/sh-PD-L1 cells were microinjected into the left or right striatum of Balb/c nude mice for 24 d. Bioluminescence imaging in living mice clearly showed that EGFP signals were invisible in right brain with U87MG/sh-PD-L1 implantation while EGFP signals were visible in both left brains with U87MG/sh-NC implantation (Fig. 1A and Fig. S3A). Reimaging of isolated mouse brains confirmed that EGFP signals were in left hemispheres (U87MG/sh-NC) but not in the right hemispheres (U87MG/sh-PD-L1) (Fig. 1B and Fig. S3B). H&E staining of brain slices further confirmed the successful xenografts formation of U87MG/sh-NC but none of U87MG/sh-PD-L1 (Fig. 1C and Fig. S3C). Statistical analysis demonstrated that the average radiance (photons/s/cm^2/sr) of U87MG/sh-PD-L1 xenograft was significantly decreased both in living mice (Fig. 1D) or isolated mouse brains (Fig. 1E) compared to U87MG/sh-NC control. These data demonstrated the oncogenic property of PD-L1 in GBM cells in vivo.

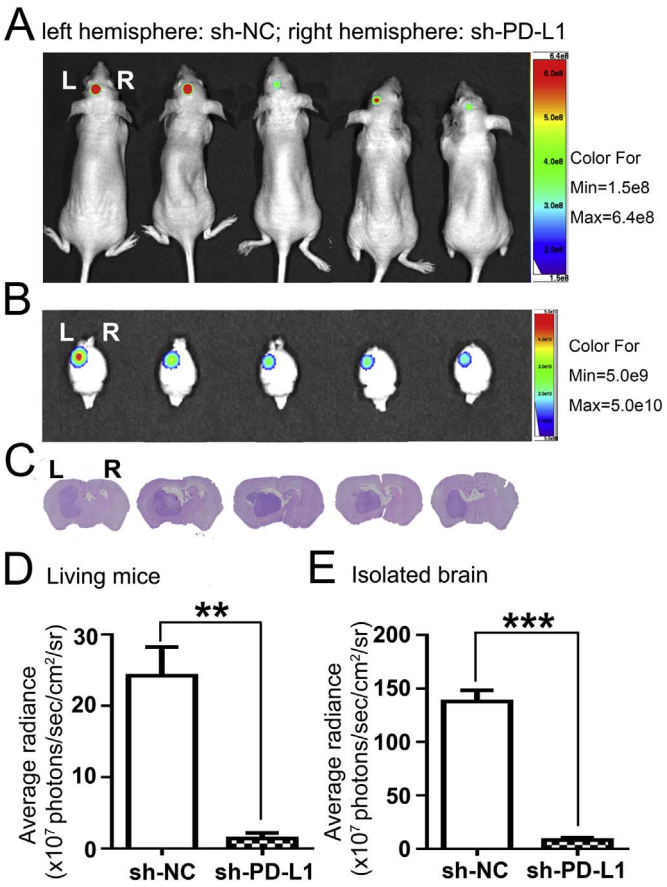

Fig. 1. PD-L1 knockdown abolishes GBM development in mouse brain. PD-L1 in human GBM U87MG cells were knocked down by lentiviral infection (LV-sh-PD-L1, with EGFP tag). Equal amounts of U87MG/LV-sh-NC (negative control) cells or U87MG/sh-PD-L1 cells were microinjected to the left or right striatum of Balb/c nude mice. (A) EGFP bioluminescence imaging of living mice after 24 d of GBM cell implantation. The intensity and range of EGFP signal in left (sh-NC) or right (sh-PD-L1) hemisphere represented corresponding tumor size. (B) EGFP bioluminescence imaging of isolated brains. After living imaging, the mice were perfused with 4% PFA and whole brains were isolated and reimaged. (C) Representative brain slices of H&E staining showed tumor size of 5 corresponding brains in (B). (D–E) Statistical analysis demonstrated the average radiance (photons/s/cm2/sr) of EGFP signals in U87MG/sh-PD-L1 xenografts was significantly decreased both in living mice (D) or isolated mouse brains (E). $^{**}P < 0.01$, $^{***}P < 0.001$ ($n = 9$).

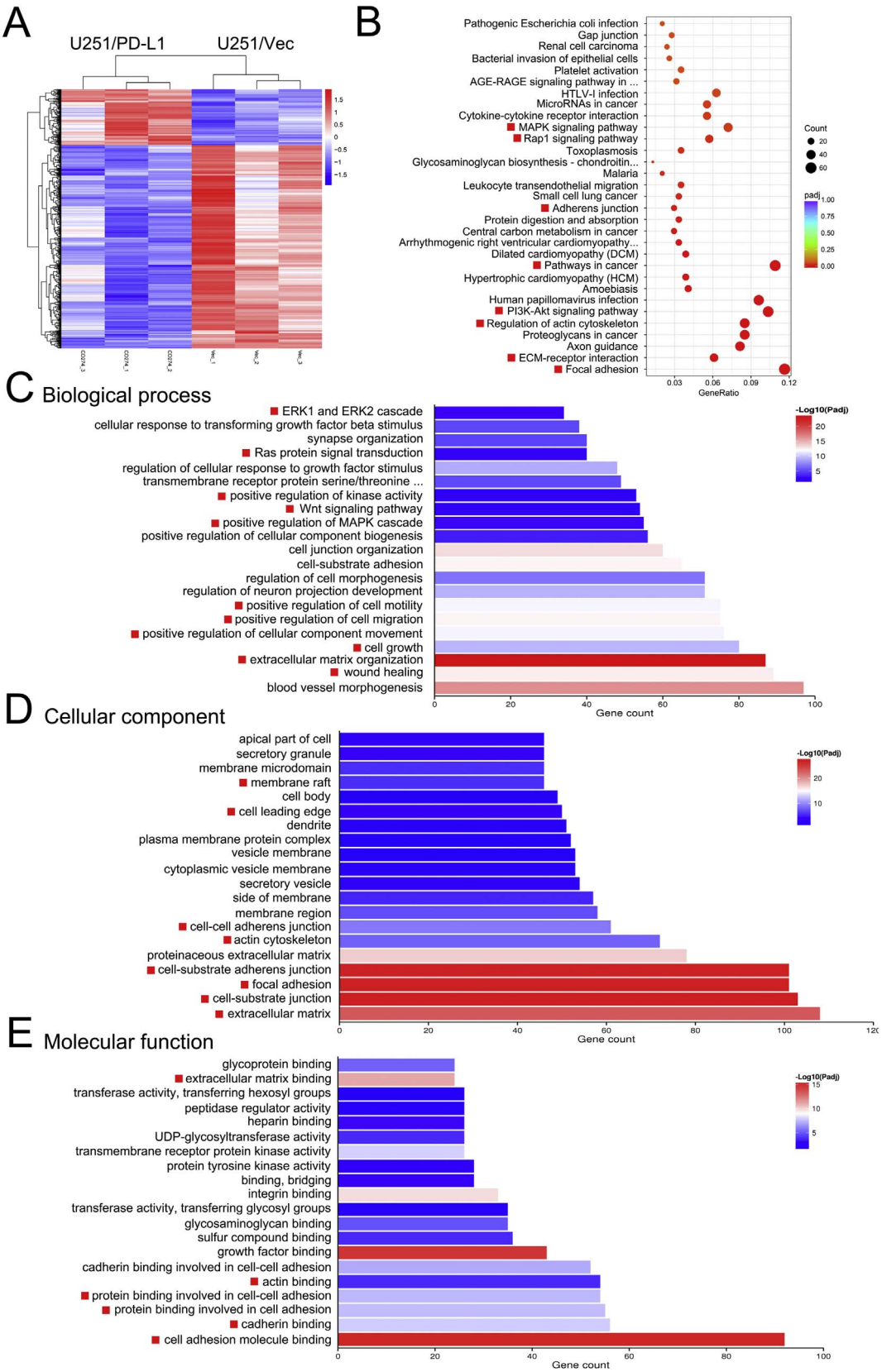

Fig. 2. Transcriptomic analysis in PD-L1-overexpressed GBM cells. (A) Differential expressed genes (DEGs) between U251/Vec and U251/PD-L1 cells. PD-L1 was overexpressed stably in human GBM U251 cells by lentiviral infection (U251/PD-L1). Total RNA was extracted from U251/PD-L1 or its control (U251/Vec) cells and subjected to mRNA-sequencing. Hot map showed significant DEGs between U251/PD-L1 and U251/Vec groups. $P < 0.005$, Padj < 0.05 and absolute fold change ≥ 1.2 ($n = 3$). (B) KEGG pathway enrichment analysis demonstrated DEGs are enriched in *Focal adhesion*, *ECM-receptor interation*, *PI3K-Akt signaling pathway*, *MAPK signaling pathway* and *Pathways in cancer* (Padj < 0.05). (C-E) Gene ontology enrichment analysis of biological process, cellular component and molecular function based on DEGs (Padj < 0.05). (C) Bar chart showed the top 21 enriched biological process items. Most of them (e.g., *wound healing*, *extracellular matrix organization*, *positive regulation of cell migration* and *positive regulation of MAPK cascade*, indicated by red squares) were involved in cancer cell migration/invasion. (D) Bar chart showed the top 20 enriched cellular component items and cell migration/invasion-related items were indicated by red squares. (E) Bar chart showed the top 20 enriched molecular function items and cell migration/invasion-related items were indicated by red squares.

3.2. PD-L1 differentially alteres gene expression enriched mainly in cell proliferation, migration and invasion pathways in GBM cells

To explore potential cellular functions and mechanisms of intrinsic PD-L1 in GBM, we performed total mRNA-sequencing using PD-L1 overexpressing GBM cells (U251/PD-L1 and U251/Vec) and systemically analyzed their gene expression profiles. Differential expressed genes (DEGs) between U251/PD-L1 and U251/Vec cells were selected by three criteria (i.e., $P < 0.005$, $P\text{adj} < 0.05$ and absolute fold change ≥ 1.2) and the selected DEGs were used for the following pathway analyses (Fig. 2A and Fig. S4). Kyoto Encyclopedia of Genes and Genomes (KEGG) pathway analysis ($P\text{adj} < 0.05$) (Table S1) revealed that these DEGs were significantly enriched in the *Focal adhesion* (gene count 63), *ECM-receptor interaction* (gene count 33), *regulation of actin cytoskeleton* (gene count 46), *Adherens junction* (gene count 16) and *Gap junction* (gene count 15) (Fig. 2B), which were heavily associated with cell migration and invasion. In addition, these DEGs were also highly enriched in *Pathway in cancer* (gene count 59), *PI3K-Akt signaling pathway* (gene count 56), *Proteoglycans in cancer* (gene count 46), *MAPK signaling pathway* (gene count 39) and *Rap1 signaling pathway* (gene count 31) (Fig. 2B), both correlating with cancer malignancy.

Gene ontology enrichment analysis (Table S2) displays DEGs in the biological process, cellular component and molecular function. Fig. 2C showed the most enriched 21 items in the biological process converged from DEGs. The most enriched items were *blood vessel morphogenesis* (gene count 97), *wound healing* (gene count 89), *extracellular matrix organization* (gene count 87), *cell growth* (gene count 80) and *positive regulation of cellular component movement* (gene count 76), which are highly associated with migration and invasion (Fig. 2C). The enrichment of PD-L1-altered DEGs in *positive regulation of MAPK cascade*, *Ras protein signal transduction*, and *Erk1 and Erk2 cascade* indicated a major role of PD-L1 in regulating Ras-MAPK signaling (Fig. 2C).

Fig. 2D and E showed the top 20 enriched items of PD-L1-altered DEGs in the cellular component and molecular function. The most enriched items in the cellular component were *extracellular matrix* (gene count 108), *cell-substrate junction* (gene count 103), *focal adhesion* (gene count 101) and *cell-substrate adherens junction* (gene count 101), which are involved in the modulation of migration process (Fig. 2D). In the molecular function, the most enriched item was *cell adhesion molecule binding* (gene count 92) (Fig. 2E), which is also associated with cancer cell migration and invasion. Taken together, our enrichment analyses revealed that intrinsic PD-L1 was heavily involved in GBM cell proliferation, migration and invasion.

3.3. Intrinsic PD-L1 promotes GBM cell proliferation

Both orthotopic GBM model experiments (Fig. 1) and transcriptomic data indicated intrinsic PD-L1 was highly associated with tumor growth or cell proliferation (Fig. 2), we then examined the effects of PD-L1 on proliferation of various human GBM cells (LN229, U251, U87MG) using PD-L1 overexpression and knockdown/knockout stable cell lines. Western blotting analysis validated PD-L1 overexpression in stable LN229/PD-L1, U251/PD-L1 and U87MG/PD-L1 cell lines compared to corresponding LN229/Vec, U251/Vec or U87MG/Vec controls (Fig. 3A). MTT assay demonstrated that PD-L1 overexpression significantly increased cell viability in LN229/PD-L1 (Fig. 3B) and U251/PD-L1 (Fig. 3C) after 3–5 d-incubation compared to corresponding LN229/Vec or U251/Vec controls. Consistently, EdU-incorporation assay demonstrated that PD-L1 overexpression significantly increased the percentage of EdU-positive cells in LN229/PD-L1 (Fig. 3D) and U87MG/PD-L1 (Fig. 3E) at 24 h of normal incubation compared to corresponding LN229/Vec or U87MG/Vec controls.

We further studied the effects of endogenous PD-L1 on GBM cell proliferation. Stable cell lines with PD-L1 knocking out and knocking down was established using CRISPR/Cas9 or RNA-interfering technique correspondingly. Western blotting analysis showed that endogenous PD-L1 was prominently decreased in stable U251/sg-PD-L1 (i.e., PD-L1 knockout, single clone; Fig. 3F and Fig. S5A), U87MG/sg-PD-L1 (i.e., cell pool; Fig. 3F and Fig. S5A), U251/sh-PD-L1 (Fig. 3G and Fig. S5B), U87MG/sh-PD-L1 (Fig. 3G and Fig. S5B) compared to corresponding sg-GFP or sh-NC controls. MTT assay demonstrated that knocking out PD-L1 in U87MG cells by either sg-PD-L1#2 or sg-PD-L1#3 significantly decreased cell viability after 3 d of normal incubation compared to sg-GFP control (Fig. 3H). We further examined the effect of PD-L1 on cell division using EdU-incorporation assay and found that PD-L1 knockout reduced EdU-positive U87MG cells (Fig. 3I–J) and knockdown reduced EdU-positive U251 cells (Fig. 3I and Fig. 3H) compared to the corresponding controls. These data together demonstrated that tumor cell-intrinsic PD-L1 facilitated GBM cell proliferation in vitro.

3.4. Intrinsic PD-L1 promotes GBM cells migration

Gene enrichment analysis revealed that PD-L1-altered signaling pathways were highly associated with cell migration and invasion (Fig. 2). Therefore, we performed scratch-wound healing assay to ask whether intrinsic PD-L1 affects GBM cell-migrating ability. After scratching, cells along the wound-edge would migrate into the nude space continuously so that the wound size, as indicated by the distance between the opposite cell-edge lines, becomes shorter over time. Compared to LN229/Vec, LN229/PD-L1 cells overexpressing PD-L1 showed apparent increasing migrating-speed at 8, 16 and 24 h after scratching as indicated by the narrower distance of opposite cell-edge lines (Fig. 4A, left panel). Statistical analysis demonstrated that the wound sizes of LN229/PD-L1 cultures were significantly reduced at 8, 16 and 24 h after scratching compared to that of LN229/Vec (Fig. 4A, right panel). In U251/PD-L1 cells, the wound sizes were also significantly reduced at 4 and 8 h after scratching compared to its Vec controls (Fig. 4B). On the contrary, U251/sg-PD-L1#2 and U251/sg-PD-L1#3 (PD-L1 knockout) cultures exhibited prominently increased wound size at 8 h after scratching compared to sg-GFP control (Fig. 4C). Consistently, U251/sh-PD-L1 (PD-L1 knockdown) also exhibited significant increased wound size at 8 and 16 h after scratching compared to corresponding sh-NC controls (Fig. 4D). Moreover, transwell assays demonstrated that PD-L1 overexpression in U251 cells (U251/PD-L1) significantly increased migrated cells compared to U251/Vec control (Fig. 4E). Taken together, we demonstrated that intrinsic PD-L1 positively regulated GBM cell migration ability.

3.5. PD-L1 activates epithelial mesenchymal transition (EMT) in GBM cells

The fact that PD-L1 knockout/knockdown largely deprived U251 cell-moving ability (Fig. 4E and G) strongly suggested a major function of intrinsic PD-L1 on controlling GBM cell migration/invasion, so we further explored the underlying mechanism. After scratching, U251/sh-NC cell along the scratch-edge (indicated by the square boxes, Fig. 5A) underwent prominent morphological alterations with prolonged pseudopodia while U251/sh-PD-L1 cell morphology did not altered significantly. Statistical analysis demonstrated that cellular longitude (Fig. 5B) and pseudopodia length (Fig. 5C), but not cellular width (Fig. 5D) of U251/sh-PD-L1 cells along scratch-edge, were significantly decreased compared to that of the U251/sh-NC control. To elucidate the underlying mechanism, we examined the effects of PD-L1 on the expression levels of EMT markers, which are pivotal in controlling cancer cell invasion/metastasis via cell transformation [37]. Western blotting analysis clearly showed that PD-L1 overexpression in U251 cells (U251/PD-L1) prominently downregulated *E*-Cadherin (epithelial marker), upregulated N-Cadherin, vimentin (mesenchymal markers) and β-catenin and Slug (upstream transcriptional factors) compared to the corresponding Vec controls (Fig. 5E). Statistical analysis demonstrated that the relative expression level of *E*-Cadherin was significantly decreased while that of N-Cadherin, vimentin, β-catenin and Slug was significantly increased in U251/PD-L1 cells compared to U251/Vec

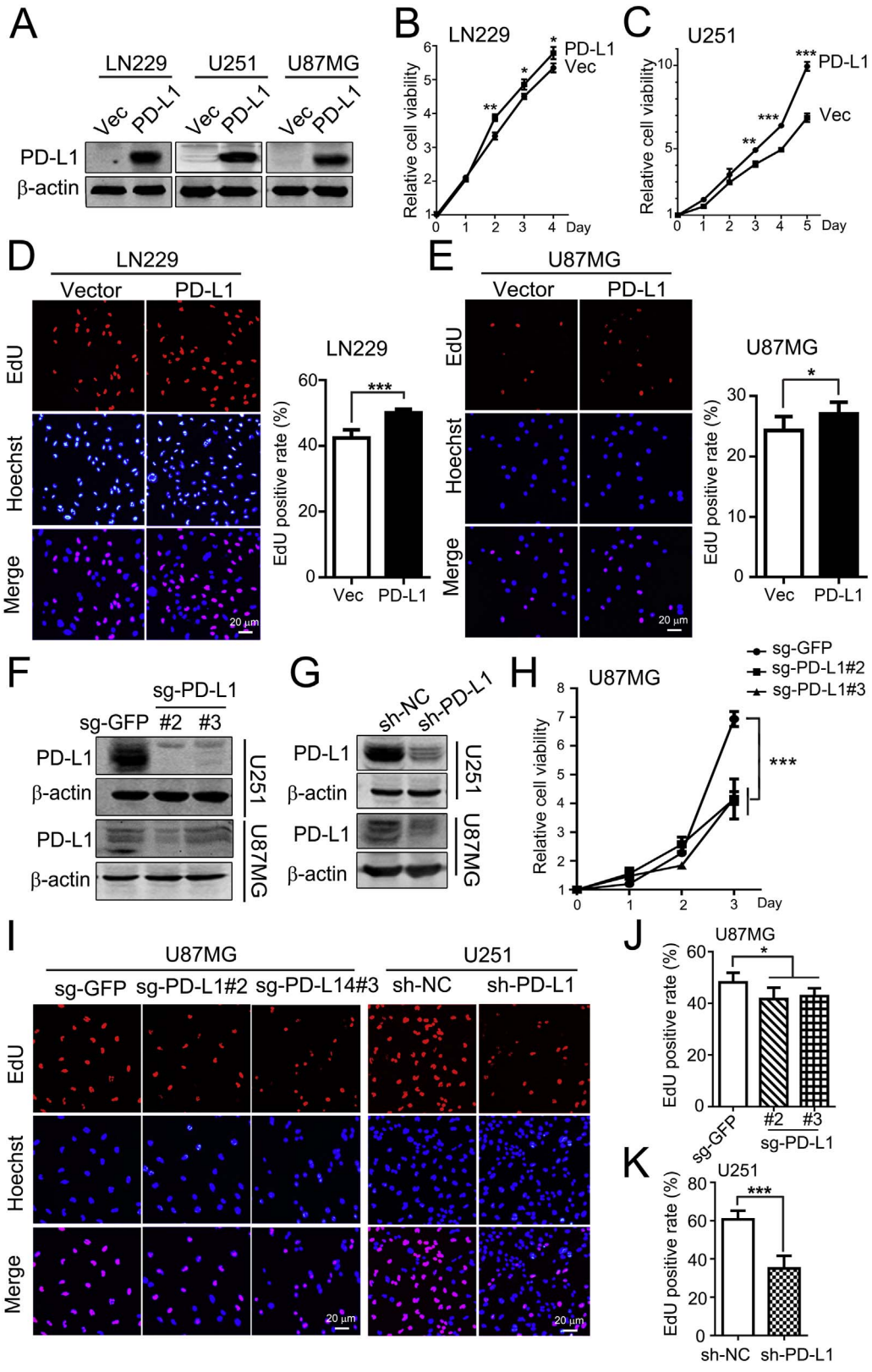

Fig. 3. PD-L1 promotes GBM cell proliferation. (A) Validation of PD-L1 overexpression of in LN229/U251/U87MG cells by Western blot analysis. (B–C) MTT assays demonstrated that PD-L1 overexpression promoted LN229 and U251 cell proliferation. $^{*}P < 0.05$, $^{**}P < 0.01$, $^{***}P < 0.001$ ($n = 6$). (D–E) Representative micrographs (left panel) and statistical analysis (right panel) of EdU-incorporation assay demonstrated that PD-L1 overexpression increased cell proliferation in LN229 and U87MG cells. $^{*}P < 0.05$, $^{***}P < 0.001$ ($n = 3$). (F) Knockout of PD-L1 via CRISPR/Cas9 technique in U251 and U87MG cells was validated by Western blot analysis. (G) Knockdown of PD-L1 via RNA interfering technique in U251 and U87MG cells was validated by Western blot analysis. (H) PD-L1 knockout significantly reduced proliferation of U87MG cells as monitored by MTT assay. $^{***}P < 0.001$ (n = 6). (I–K) Representative micrographs (I) and statistical analysis (J–K) of EdU-incorporation assay demonstrated that knockout and knockdown of PD-L1 decreased cell proliferation in U87MG/sg-PD-L1 and U251/sh-PD-L1 cells respectively. $^{*}P < 0.05$, $^{***}P < 0.001$ ($n = 3$).

cells (Fig. 5F). Consistently, immunofluorescent staining demonstrated that PD-L1 knockdown (U251/sh-PD-L1, with EGFP tag) evidently reduced vimentin in U251 cells along the scratching edge compared to U251/sh-NC (Fig. 5G).

3.6. PD-L1 activates epithelial mesenchymal transition (EMT) via MEK-Erk-dependent signaling

It is known that MEK/Erk and PI3K/Akt cascade promotes EMT by upregulating Slug and β-catenin through GSK-3β-dependent or GSK-3β-independent pathways [38,39]. In addition, PD-L1 overexpression

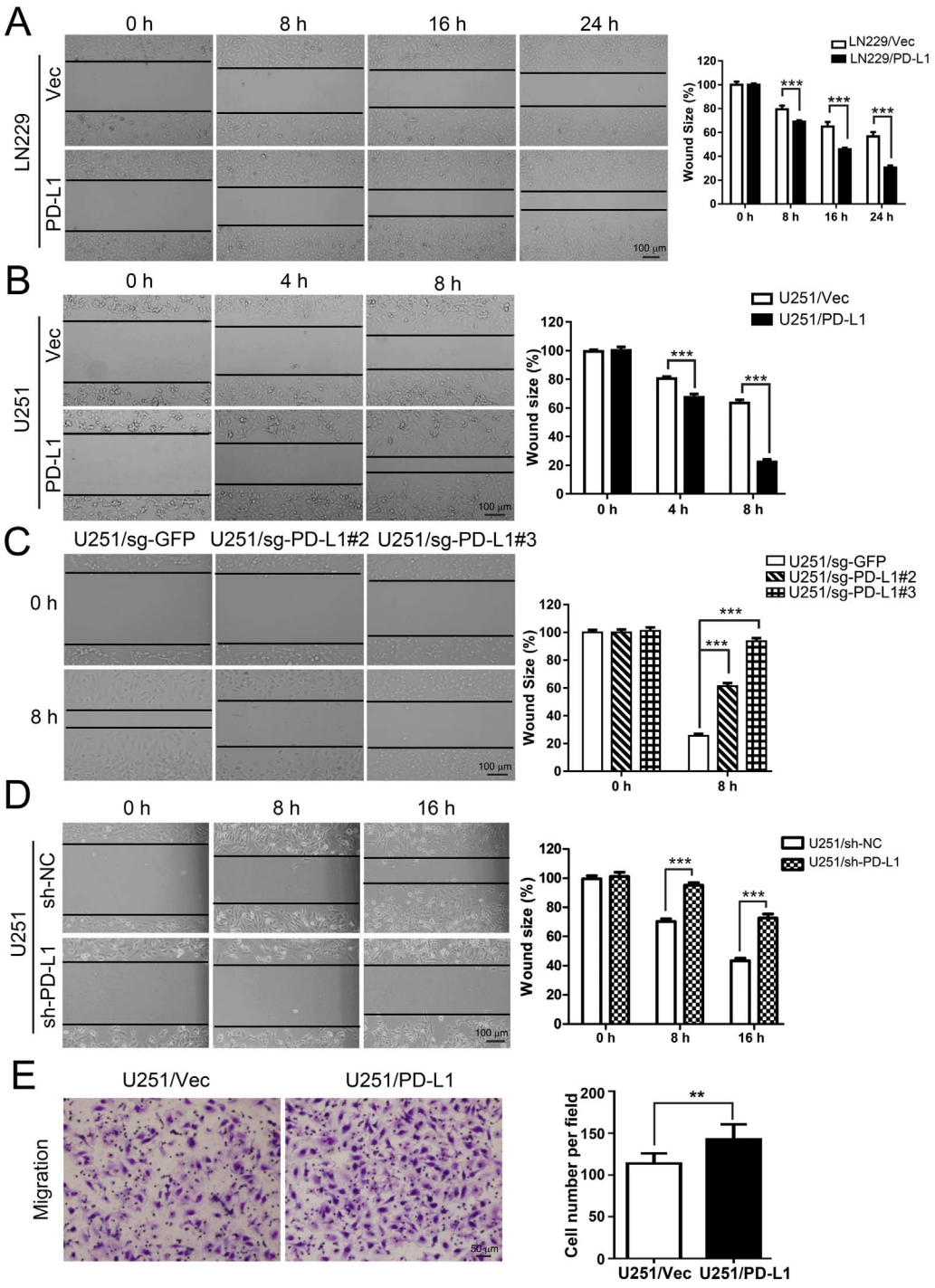

Fig. 4. PD-L1 promotes GBM cell migration. Cell migration was monitored by scratch wound-healing assay in GBM cells with FBS withdrawal. (A) Representative micrographs and statistical analysis demonstrated PD-L1 overexpression significantly reduced wound size in LN229 cell cultures at 8, 16 and 24 h after scratching. $^{***}P < 0.001$ ($n = 3$). (B) Representative micrographs and statistical analysis demonstrated PD-L1 overexpression significantly reduced wound size in U251 cell cultures at 4 and 8 h after scratching. $^{***}P < 0.001$ ($n = 3$). (C) Representative micrographs and statistical analysis demonstrated that PD-L1 knockout (sg-PD-L1#2 and #3) significantly increased wound size in U251 cell culture at 8 h after scratching. $^{***}P < 0.001$ (n = 3). (D) Representative micrographs and statistical analysis demonstrated that PD-L1 knockdown (sh-PD-L1) significantly increased wound size in U251 cell cultures at 8 and 16 h after scratching. $^{***}P < 0.001$ (n = 3). (E) Representative micrographs and statistical analysis demonstrated that PD-L1 overexpression significantly increased migrated U251 cells in transwell assays. $^{**}P < 0.01$ (n = 3).

notably altered MAPK and PI3K-Akt signaling pathways (Fig. 2B), and Erk1/2-associated biological processes (Fig. 2C). Western blotting analysis demonstrated that PD-L1 overexpression selectively increased p-Erk1/2 but not p-Akt or p-GSK-3β (Fig. 6A). Statistical analysis demonstrated that p-Erk1/T-Erk1, p-Erk2/T-Erk2 and T-Akt/β-actin were significant increased, p-Akt/T-Akt was significantly decreased, while p-Akt/β-actin and p-GSK-3β/T-GSK-3β remained unaltered in U251/PD-L1 cells compared to U251/Vec (Fig. 6B). These evidences demonstrated that PD-L1 selectively activated Erk but not Akt or GSK-3β.

The selective involvement of MEK-Erk signaling in PD-L1-induced EMT was further demonstrated using specific pharmacological inhibitors. Western blot and statistical analysis demonstrated that U0126 (20 μM, MEK1/2 inhibitor) treatment significantly reversed PD-L1-altered expression of Slug, vimentin, N-Cadherin and *E*-Cadherin in U251/PD-L1 cells (Fig. 6C–D). However, LY294002 (25 μM, PI3K inhibitor, Fig. 6E–F) and SB415286 (20 μM, GSK-3α/β inhibitor, Fig. S6) had no obvious effects on reversing PD-L1-altered Slug, vimentin, E-Cadherin or N-Cadherin in U251 cells. Taken together, our results showed that PD-L1 upregulated EMT key molecules via MEK/Erk selectively.

3.7. PD-L1 binds to and activates Ras

Since PD-L1 overexpression exhibited a striking effect on Erk activation (Fig. 6A), it was interesting to study through which mechanisms PD-L1 activated Erk. As Ras-MEK-Erk is the canonical pathway for Erk

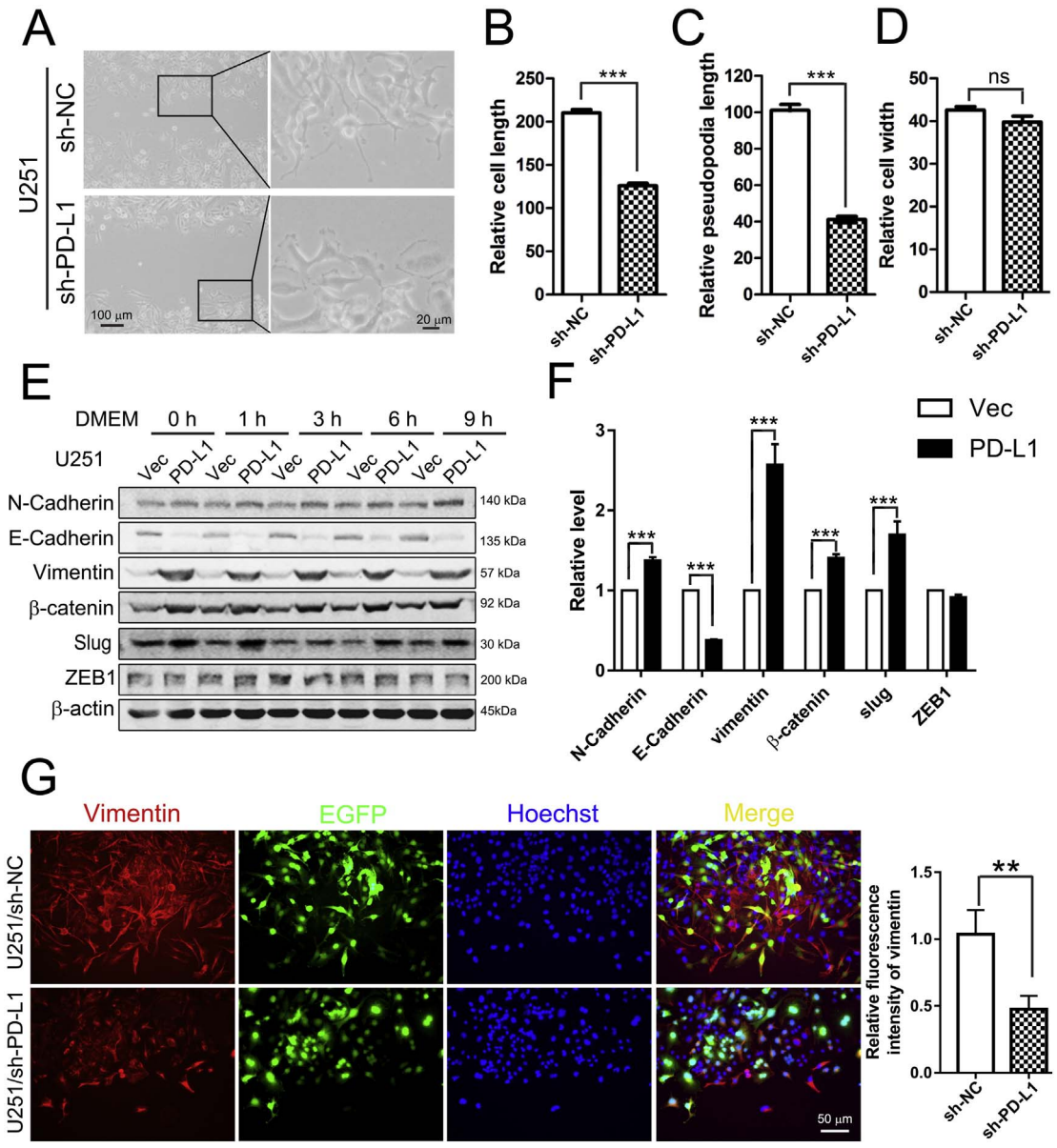

Fig. 5. PD-L1 activates epithelial mesenchymal transition (EMT) process in GBM cells. (A–D) PD-L1 knockdown abolished scratching-stimulated cell transformation in U251 cells. Representative micrographs showed that migrating U251/sh-NC (upper panels) but not U251/sh-PD-L1 (lower panels) cells extended evident pseudopodia after 16 h of scratching. Related morphologic parameters of migrating cells were measured. Statistical analysis demonstrated that cell length (B) and pseudopodia length (C) but not cell width (D) were significantly reduced in U251/sh-PD-L1 cells compared to U251/sh-NC control cells. ***$P < 0.001$ ($n = 3$). ns, no significance. (E–F) Western blot detected the expression of EMT marker proteins in PD-L1-overexpressed U251 cells. Confluent U251/Vec and U251/PD-L1 cells were treated with serum-free DMEM for various time and subjected to Western blot analysis. Representative Western blot (E) and statistical analysis (F) demonstrated N-Cadherin, vimentin, β-catenin and Slug were significantly upregulated while E-Cadherin was downregulated in U251/PD-L1 cells compared to U251/vec control cells. ***$P < 0.001$ ($n = 3$). (G) Results of fluorescent immunostaining demonstrated that vimentin was significantly downregulated in U251/sh-PD-L1 cells compared to U251/sh-NC cells. **$P < 0.01$ (n = 3).

activation [40], we proposed that PD-L1 might activate Erk through Ras-MEK-Erk signaling. GST-pull down assay clearly showed that H-Ras bound to PD-L1 in both 293 T (Fig. 7A) and LN229 (Fig. 7B) cells that were co-transfected with GST-H-Ras + PD-L1 or GST + PD-L1. Further, we demonstrated that H-Ras bound to endogenous PD-L1 in LN229 cells with GST-H-Ras/GST overexpression alone (Fig. 7C). We also detected significant increase of active Ras (GTP-bound Ras) in U251/PD-L1 cells compared to U251/Vec cells although less total Ras was presented (Fig. 7D). These data demonstrated that PD-L1 directly bound Ras and played a major role in Ras activation, subsequently led to Erk activation.

As the role of PD-L1-Ras-MEK/Erk-EMT signaling was revealed, we then verified the functional role of MEK/Erk in GBM cell-migration upon PD-L1 overexpression. Scratch-wound assay found that pharmacological inhibition of MEK/Erk by U0126 completely abolished PD-L1-promoted cell migration (Fig. 7E) or wound-healing (Fig. 7F) in LN229/PD-L1 compared to LN229/Vec. Further, EdU-incorporation assay demonstrated that pharmacological inhibition of Erk1/2 by SCH772984 (a specific Erk1/2 inhibitor) completely blocked PD-L1-enhanced cell proliferation in U251 cells (Fig. 7G). Thus, we confirmed that PD-L1 activated EMT via Ras-MEK/Erk signaling.

3.8. PD-L1 activates EMT and promotes GBM development and invasion in orthotopic GBM model of rats

Finally, to further verify our in vitro findings, we studied the roles of PD-L1 in GBM development and invasion in in vivo models. Equal amounts of rat glioma C6 cells stably overexpressing PD-L1 (C6/PD-L1)

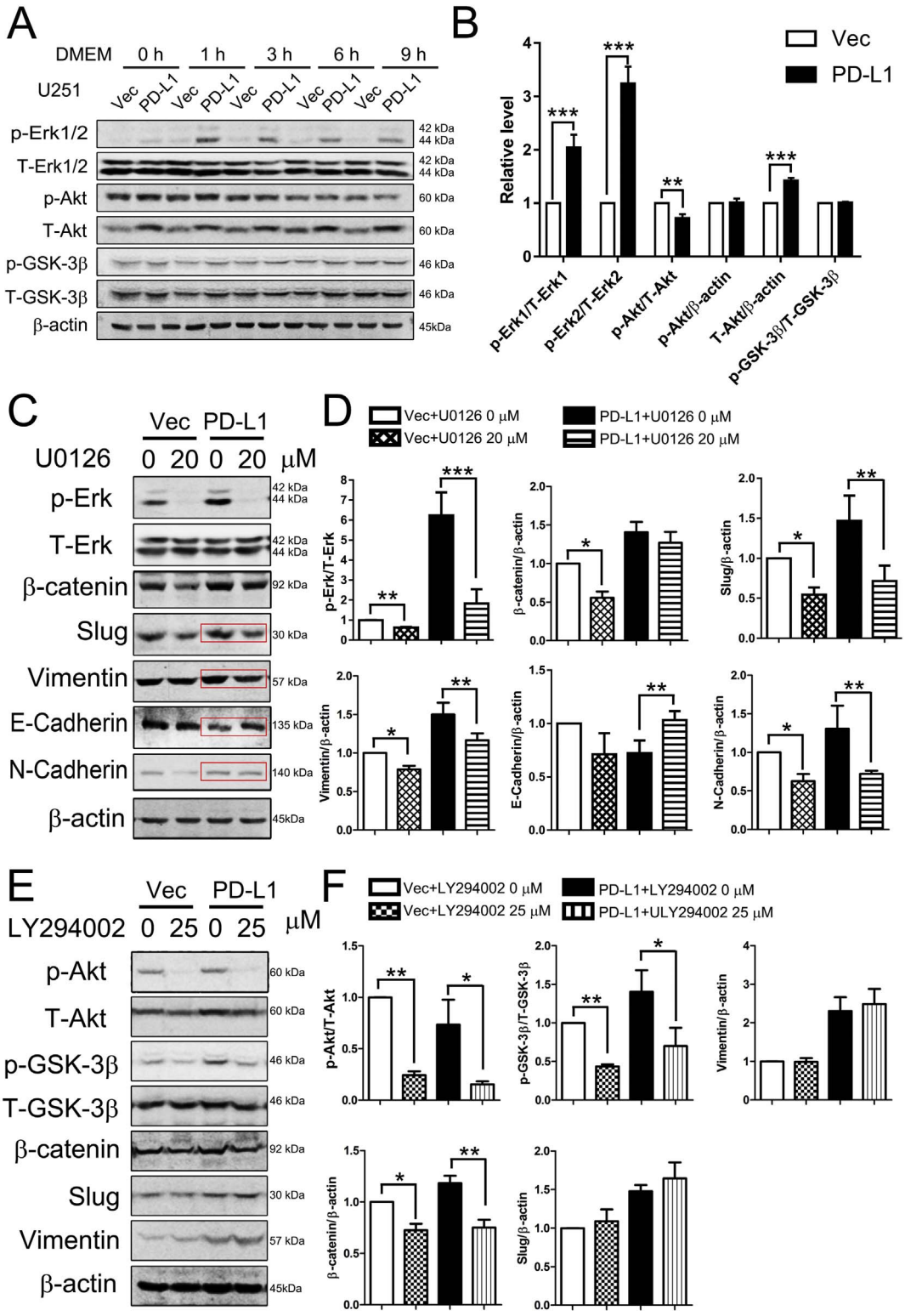

Fig. 6. PD-L1 activates EMT via MEK-Erk-dependent signaling. (A–B) Western blot (A) statistical analysis (B) demonstrated that PD-L1 overexpression in U251 significantly upregulated p-Erk1/2 but not p-Akt or p-GSK-3β compared to the corresponding Vec control. $^{**}P < 0.01$, $^{***}P < 0.001$ (n = 3). (C–D) Western blot (C) and statistical analysis (D) demonstrated that pharmacological inhibition of MEK by U0126 (20 μM) suppressed Slug/vimentin or increased E-cadherin in U251 cells upon PD-L1 overexpression. Confluent U251/Vec and U251/PD-L1 cells were treated with serum-free DMEM containing 0 or 20 μM U0126 for 3 h and subjected to Western blot analysis. $^{*}P < 0.05$, $^{**}P < 0.01$, $^{***}P < 0.001$ (n = 3). (E-F) Western blot (E) and statistical analysis (F) demonstrated that inhibition of PI3K/Akt by LY294002 (25 μM) had no effect on EMT-related proteins expression upon PD-L1 overexpression. $^{*}P < 0.05$, $^{**}P < 0.01$ (n = 3).

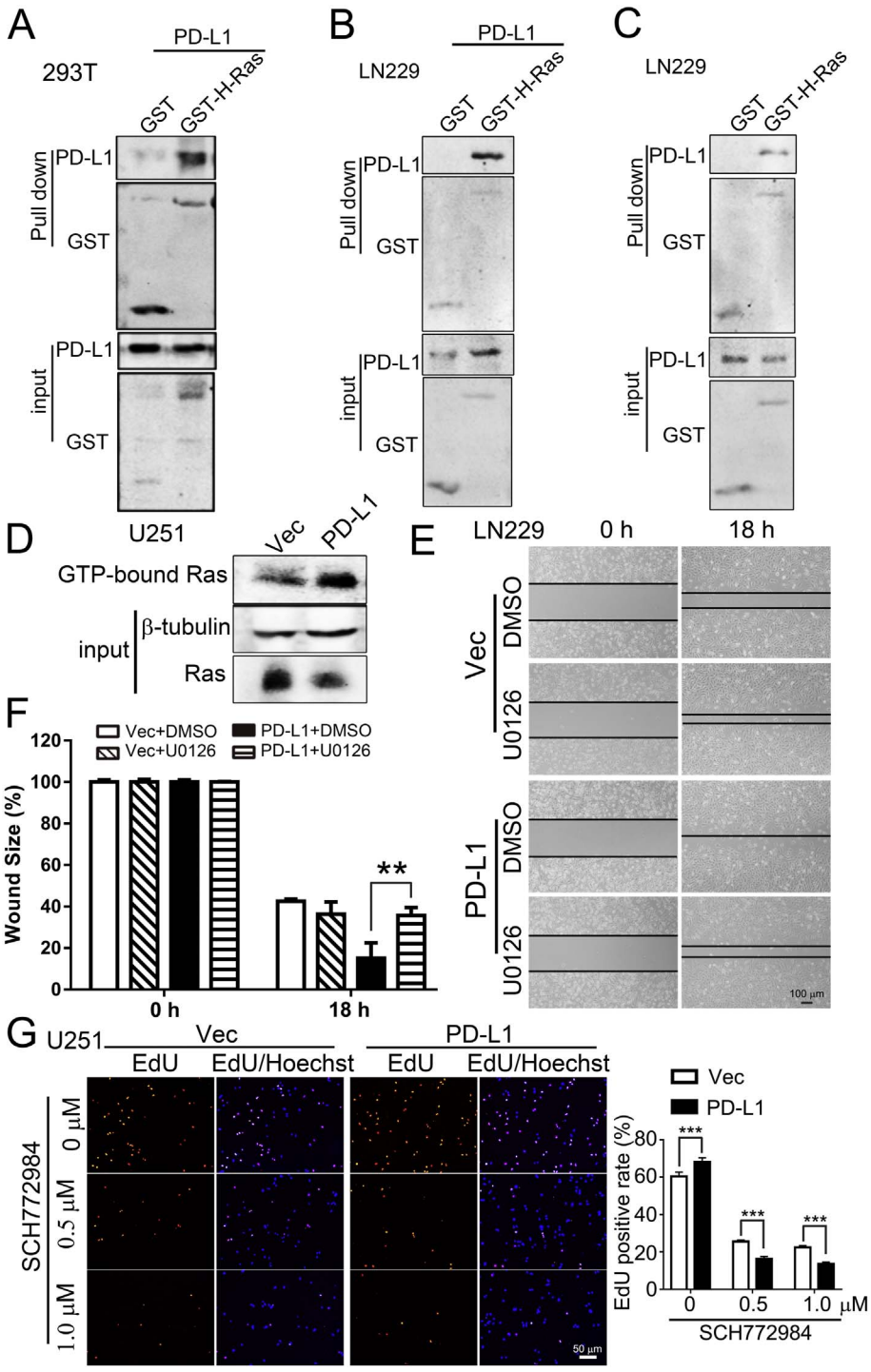

Fig. 7. PD-L1 binds to and activates Ras. (A) PD-L1 bound to H-Ras in 293 T cells. PD-L1 was co-overexpressed with GST or GST-H-Ras in 293 T cells for 24 h and 400 μg of total soluble proteins was subjected to GST-pull down assay. Results of Western blot showed that PD-L1 bound to H-Ras. (B) GST-pull down assay showed that PD-L1 bound to H-Ras in LN229 cells. (C) GST-H-Ras bound to endogenous PD-L1 in LN229 cells. GST-H-Ras or GST was overexpressed in LN229 cells and equal amount of total soluble proteins were subjected to GST-pull down and Western blotting analysis. (D) PD-L1 induced Ras activation in U251 cells. PD-L1 was overexpressed in U251 cells for 24 h. GTP-bound Ras (i.e., active Ras) was detected with corresponding antibody by Western blotting analysis. (E–F) Scratch-wound healing assay (E) and statistical analysis (F) demonstrated that U0126 significantly reduced PD-L1-promoted cell migration in LN229 cells after scratching. U0126 at 0 or 20 μM was added to cell culture immediately after scratch. $^{**}P < 0.01$ (n = 3). (G) EdU-incorporation assay and statistical analysis demonstrated that SCH772984 (specific Erk1/2 inhibitor) significantly reduced PD-L1-enhanced cell proliferation. SCH772984 was supplemented to cultures at 6 h after initial cell seeding. $^{***}P < 0.001$ (n = 3).

or the empty vector control (C6/Vec) were microinjected into right or left striatum of rat brains for 14 d. Serial brain sections were cut to cover the whole GBM tissues (Fig. 8A). H&E stained brain slices clearly showed significant larger C6/PD-L1 glioma size compared to C6/Vec (Fig. 8B–C). Notably, C6/PD-L1 glioma exhibited more invasive glioma cell colonies compared to C6/Vec control (enclosed red dot lines, right panels, Fig. 8D). Statistical analysis showed that invasive index (invasive area/tumor rim length) in C6/PD-L1 glioma was significantly increased compared to C6/Vec control (Fig. 8E). IHC of PD-L1 clearly showed a PD-L1-ringe along tumor infiltrating frontier in C6/Vec glioma (Fig. 8F). We also found that PD-L1 expression in tumor frontier was significantly higher than that of inner area (square box, Fig. 8F, right panel and Fig. 8G).

IHC analysis showed that vimentin and N-Cadherin were increased in C6/PD-L1 glioma while the *E*-Cadherin was decreased in C6/PD-L1 glioma compared to C6/Vec glioma (Fig. 9A–D). These data confirmed that PD-L1 enhanced GBM cell invasion via EMT in vivo. Double-fluorescent immunostaining showed that increased vimentin signals were strongly co-localized and correlated ($r = 0.8585$, $P < 0.0001$) with PD-L1 signals in C6/PD-L1 glioma (Fig. 9E). We further confirmed this result in human GBM tissues by demonstrating the positive correlation between PD-L1 and vimentin in human GBM slices ($r = 0.8537$, $P < 0.0001$, Fig. 9F). We thereby confirmed that PD-L1 enhanced GBM cell invasion via EMT in vivo.

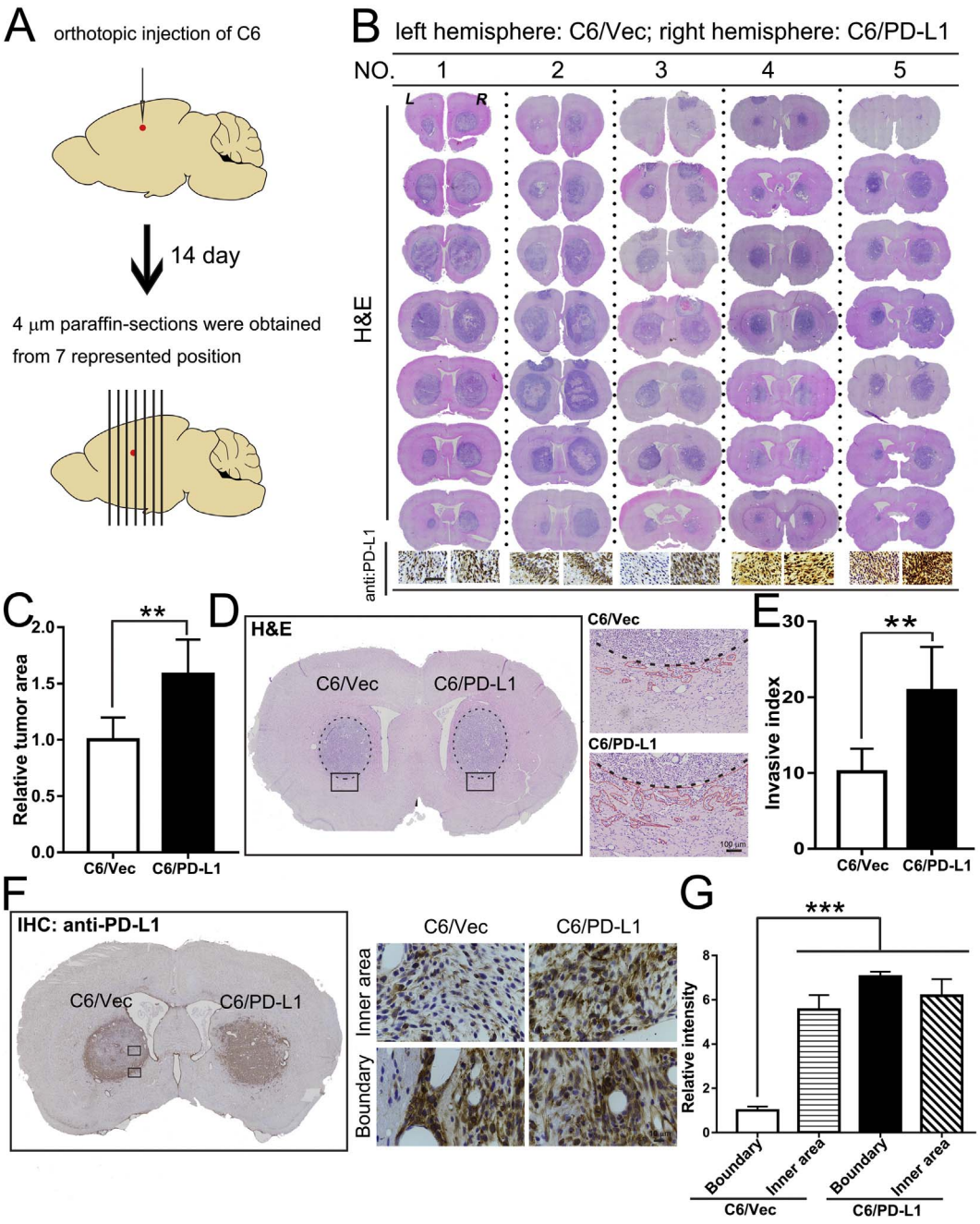

Fig. 8. PD-L1 overexpression promotes GBM development and invasion in orthotopic models of rats. Equal amounts of C6/Vec (negative control) or C6/PD-L1 GBM cells were microinjected to the left or right striatum of rats and brain tumors were analyzed after 14 d of initial implantation. (A) Schematic diagram showed the 7 representative brain slices cut from the brain (indicated by black lines, covering the whole allograft). (B) H&E staining of brain slices from 5 glioma-loading brains (7 sections/brain). Lower panels showed IHC results of PD-L1 expression of corresponding allograft in the brains. Bar, 50 μm. (C) Statistical analysis demonstrated that relative tumor area of C6/PD-L1 allografts was significantly increased compared to C6/Vec group. $^{**}P < 0.01$ ($n = 5$). (D) Representative H&E staining result showed that glioma cell invasion was increased in C6/PD-L1 allograft compared to C6/Vec control. Rectangle box in brain slice (left panel) and its enlarged micrograph (right panels) indicated the position of invasive glioma cell colonies. Tumor rim was indicated by black dash lines and invading cells was circled with red dashed dot lines. (E) Statistical analysis demonstrated that the invasive index in C6/PD-L1 allografts was significantly increased compared to C6/Vec control. The invasive index was calculated as the ratio of invading tumor area to tumor rim length. $^{**}P < 0.05$ (n = 5 tumors). (F) IHC staining of PD-L1 of intracranial glioma allografts. Left panel showed whole brain image of PD-L1 staining. Right panels showed PD-L1 staining of the inner (upper panels) and boundary of C6/Vec allograft (indicated by the rectangle boxes in the whole brain slice). (G) Statistical analysis demonstrated that PD-L1 was significantly increased in boundary tumor cells compared to inner tumor cells in C6/Vec glioma. $^{***}P < 0.001$ (n = 5).

4. Discussion

In the present study, we demonstrate a critical role of PD-L1 in conferring GBM malignancy with a variety level of studies. First, we observed that in vivo knockdown of PD-L1 in nude mice completely abolished glioma xenografts formation. Further, our bioinformatics analysis showed that PD-L1 overexpression mainly altered gene expression converged in cell migration and invasion. To experimentally demonstrate the role of intrinsic PD-L1 in GBM, we conducted a series of in vitro studies using stable PD-L1 overexpression GBM cell lines, and had identified a novel intrinsic interaction of PD-L1 with H-Ras, leading to Ras-Erk-EMT activation. To verify these in vitro findings, we microinjected glioma C6 cells overexpressing PD-L1 into rat striatum and confirmed that PD-L1 activates EMT and promotes GBM development

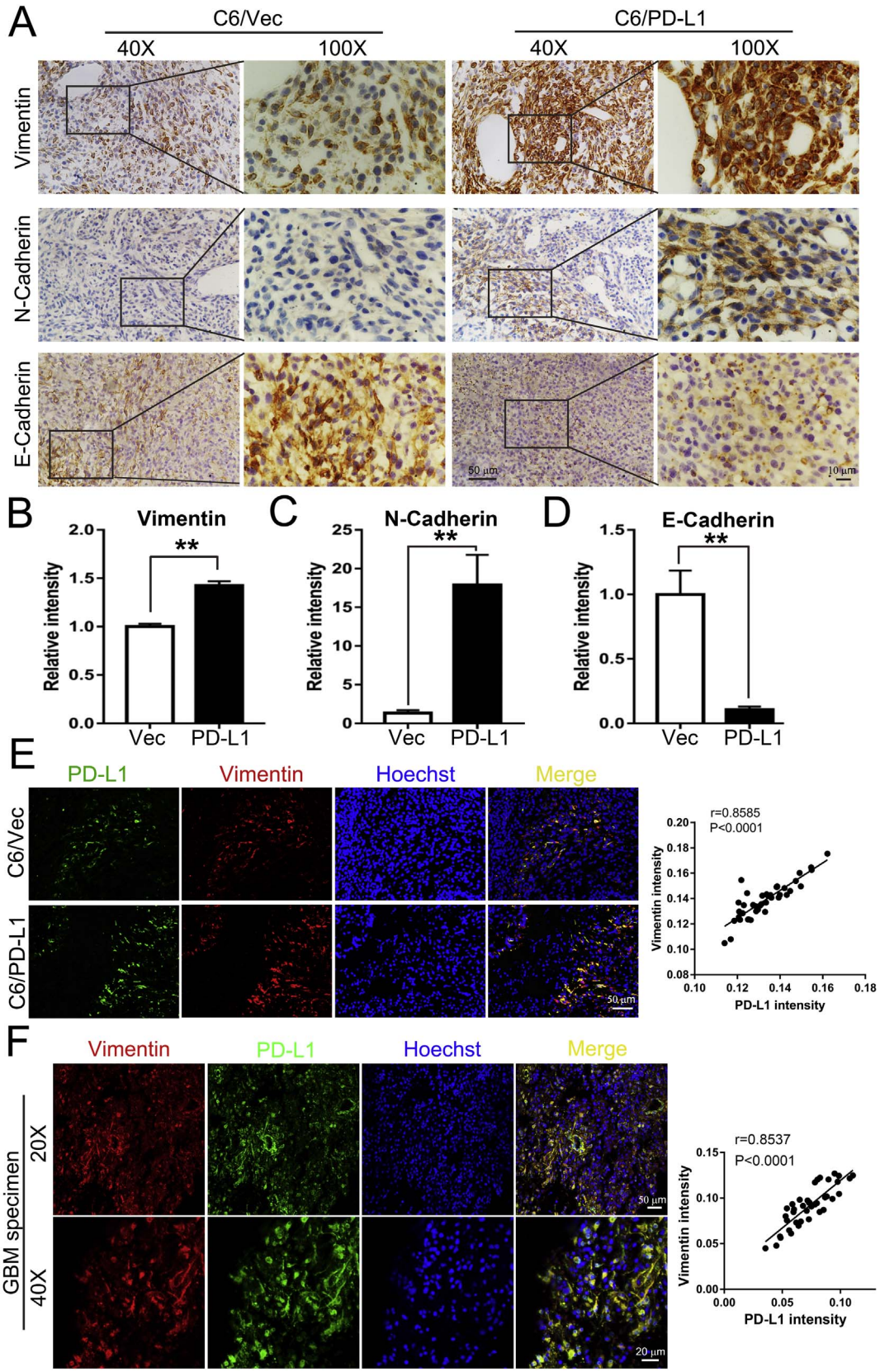

Fig. 9. PD-L1 overexpression activated EMT markers in vivo. (A) Representative micrographs of vimentin, N-Cadherin and E-Cadherin staining (IHC) of intracranial C6/Vec and C6/PD-L1 allografts in SD rats. (B–D) Statistical analysis demonstrated that PD-L1 overexpression enhanced vimentin (B) and N-Cadherin (C), and decreased E-Cadherin (D) expression. $^{**}P < 0.01$ (n = 5). (E) Double-fluorescent immunostaining of vimentin and PD-L1 of glioma allografts in SD rats (upper panel, C6/Vec; lower panel, C6/PD-L1). Statistical analysis demonstrated the positive correlation between PD-L1 and vimentin (r = 0.8585, $P < 0.0001$). (F) Double-fluorescent immunostaining of vimentin and PD-L1 in GBM specimen from patient. Statistical analysis demonstrated the positive correlation between PD-L1 and vimentin (r = 0.8537, $P < 0.0001$).

and invasion. Lastly, we translated our animal studies in human GBM tissues, further reinforcing that PD-L1 could enhance GBM cell invasion via EMT.

We first explored the biological functions of intrinsic PD-L1 in cancer cells via transcriptome-based bioinformatics. Immune therapy targeting to PD-1/PD-L1 pairs has achieved revolutionary results in many malignant tumors such as melanoma and non-small cell lung cancer [5,41]. However, results of anti-PD-1/PD-L1 therapy in GBM patients remain unreported, probably reflecting the difficulty in GBM treatment. PD-L1 expression level is highly associated to poor overall survival and becomes an important prognostic biomarker for PD-L1 antibody-based immune therapy in various cancers including melanoma [41].

In glioma, high PD-L1 expression was associated with worsening of overall survival, as suggested by a meta-analysis [23] and a database-based analysis from The Cancer Genome Atlas [25]. However, PD-L1 is also reported to have no correlation with patient overall survival [42], indicating complicated biological functions of PD-L1 in GBM. It is well-known that PD-L1 mediates immune cell response via canonical PD-L1/PD-1 interaction, while recent studies found that intrinsic PD-L1 also plays an important role in tumorigenesis, suggesting that intracellular PD-L1 is also a potential therapeutic target [17,18]. To search key biological function of intrinsic PD-L1, we performed systemic mRNA-sequencing in PD-L1-overexpressed GBM cells and found that PD-L1-altered gene expression was largely enriched in cellular process of migration and invasion. The effects of PD-L1 on promoting GBM cell migration and invasion in vitro and in vivo were further demonstrated by PD-L1 overexpression and knockdown/knockout techniques. Notably, knocking down or out intrinsic PD-L1 nearly abolished GBM cell migration in cell-scratching model (Fig. 4C and D). Consistently, PD-L1 knockdown completely abolished orthotopic U87MG-xenografts in nude mice (Fig. 1). These evidences strongly demonstrated a major function of intrinsic PD-L1 in cancer cell proliferation, migration and invasion.

We clarified that PD-L1 promoted GBM cell migration and invasion by inducing EMT, a key step required for reshaping cell so as to move [37]. The lack of typical pseudopodia in U251/sh-PD-L1 cells after scratching-stimuli proved that PD-L1 controlled GBM cell-transformation (Fig. 5A). Database analysis demonstrated that PD-L1 expressed more in mesenchymal subtype and may contribute to a mesenchymal phenotype in glioblastoma [25,42]. Consistently, our study demonstrated that PD-L1 showed prominent effects on downregulating E-cadherin but upregulating N-cadherin, vimentin as well as their transcriptional factors (Slug, β-catenin) in vitro (Fig. 5E) and in vivo (Fig. 9A), which are the characteristic EMT events required for cell-transformation [43,44]. It is conceivable that PD-L1-inducd EMT would enhance GBM cell malignancy in vivo.

Further, we elucidated how PD-L1 promoted EMT in GBM cells. Ras/Raf/MEK/Erk and PTEN/PI3K/Akt are two major aberrant oncogenic signaling pathways in GBM [45], as well-known for regulating EMT and cancer cell migration/invasion [39]. In ovarian cancer and melanoma, PD-L1 induces PI3K/Akt activation [17], however, in U251 GBM cells, PD-L1 primarily induced a striking Erk activation (Fig. 6A). Consistently, pharmacological inhibition of MEK/Erk, but not PI3K/Akt/GSK3β signaling, abolished PD-L1-induced EMT alterations (Fig. 6C and E). Therefore, PD-L1 activated EMT pathway in a MEK/Erk dependent manner in GBM cells.

Importantly, we discovered that PD-L1 directly bound to H-Ras. Further, PD-L1 overexpression strongly increased the level of active-form Ras in GBM cells (Fig. 7). Since Ras is canonic activator for Erk activation via Ras/Raf/MEK/Erk, the binding of PD-L1 and Ras provided a reliable molecular working model for the explanation of Erk activation in GBM cells. Considering that primary oncogenic role of Ras that over 80% of GBM patients have EGFR/Ras/Raf/MEK/Erk mutation/activation [46], the binding of PD-L1 and Ras might greatly contribute to GBM development.

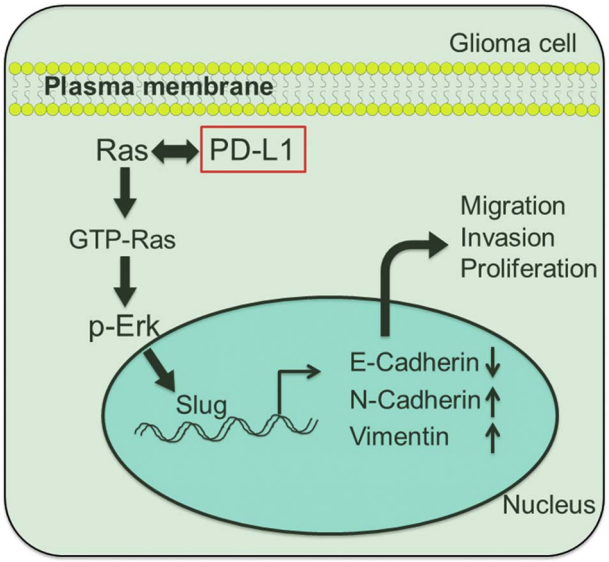

Fig. 10. Proposed role and mechanism of PD-L1 in GBM malignancy. The interaction between PD-L1 and Ras induces Ras transformed into GTP-bound active state. It subsequently activates Ras/Raf/MEK/Erk cascade, which activated epithelial mesenchymal transition (EMT). All processes finally promote GBM cell proliferation/migration/invasion. ↓ or ↑, increase or decrease; →, induction or activation; ↔, binding.

In conclusion, we identified a novel binding partner of PD-L1, Ras, and further demonstrated that PD-L1 promoted GBM development via PD-L1/Ras/Erk/EMT. We proposed that the interaction of PD-L1 and Ras induced the activation of Ras/Raf/MEK/Erk cascade, thus promoting GBM cell migration/invasion via EMT (Fig. 10). Our findings strongly suggest that targeting intrinsic PD-L1 has considerable therapeutic effect in GBM.

Transparency document

Supplementary data to this article can be found online at https://doi.org/10.1016/j.bbadis.2018.03.002.

Transparency document

The http://dx.doi.org/10.1016/j.bbadis.2018.03.002 associated with this article can be found in online version.

Acknowledgments

This work was supported by the National Nature Science Foundation of China [NO. 81672504, 81471386], the Fundamental Research Funds for the Central Universities [No. 2017KFYXJJ048], the Natural Science Foundation of Hubei Province [No. 2017CFB639] and the Integrated Innovative Team for Major Human Diseases Program of Tongji Medical College, HUST (Grant 5001530026).

Conflict of interest

The authors declare that there are no conflicts of interest.

Author contributions

XYQ and DXH performed the major experiments and analyzed the data; XYQ wrote the manuscript; WQC and RQC provided editorial suggestions and final revision of the manuscript; SRQ, YJL, CYL, FP, DL, and XXX performed some experiments or data analysis; SBY organized the experimental studies; XQC conceived and designed the study, as well as wrote the manuscript. All the authors were involved in

reviewing and commenting on the manuscript, and gave their approval of the submitted version of the manuscript.

Appendix A. Supplementary data

Supplementary data to this article can be found online at https://doi.org/10.1016/j.bbadis.2018.03.002.

References

[1] P.Y. Wen, S. Kesari, Malignant gliomas in adults, N. Engl. J. Med. 359 (2008) 492–507.

[2] R. Stupp, M.E. Hegi, W.P. Mason, M.J. van den Bent, M.J. Taphoorn, R.C. Janzer, S.K. Ludwin, A. Allgeier, B. Fisher, K. Belanger, P. Hau, A.A. Brandes, J. Gijtenbeek, C. Marosi, C.J. Vecht, K. Mokhtari, P. Wesseling, S. Villa, E. Eisenhauer, T. Gorlia, M. Weller, D. Lacombe, J.G. Cairncross, R.O. Mirimanoff, R. European Organisation for, T. Treatment of Cancer Brain, G. Radiation Oncology, G. National Cancer Institute of Canada Clinical Trials, Effects of radiotherapy with concomitant and adjuvant temozolomide versus radiotherapy alone on survival in glioblastoma in a randomised phase III study: 5-year analysis of the EORTC-NCIC trial, Lancet Oncol. 10 (2009) 459–466.

[3] B. Tran, M.A. Rosenthal, Survival comparison between glioblastoma multiforme and other incurable cancers, J. Clin. Neurosci. 17 (2010) 417–421.

[4] R. Stupp, W.P. Mason, M.J. van den Bent, M. Weller, B. Fisher, M.J. Taphoorn, K. Belanger, A.A. Brandes, C. Marosi, U. Bogdahn, J. Curschmann, R.C. Janzer, S.K. Ludwin, T. Gorlia, A. Allgeier, D. Lacombe, J.G. Cairncross, E. Eisenhauer, R.O. Mirimanoff, R. European Organisation for, T. Treatment of Cancer Brain, G. Radiotherapy, G. National Cancer Institute of Canada Clinical Trials, Radiotherapy plus concomitant and adjuvant temozolomide for glioblastoma, N. Engl. J. Med. 352 (2005) 987–996.

[5] J.D. Wolchok, PD-1 Blockers, Cell 162 (2015) 937.

[6] S. Afreen, S. Dermime, The immunoinhibitory B7-H1 molecule as a potential target in cancer: killing many birds with one stone, Hematol. Oncol. Stem Cell Ther. 7 (2014) 1–17.

[7] P.C. Tumeh, C.L. Harview, J.H. Yearley, I.P. Shintaku, E.J. Taylor, L. Robert, B. Chmielowski, M. Spasic, G. Henry, V. Ciobanu, A.N. West, M. Carmona, C. Kivork, E. Seja, G. Cherry, A.J. Gutierrez, T.R. Grogan, C. Mateus, G. Tomasic, J.A. Glaspy, R.O. Emerson, H. Robins, R.H. Pierce, D.A. Elashoff, C. Robert, A. Ribas, PD-1 blockade induces responses by inhibiting adaptive immune resistance, Nature 515 (2014) 568–571.

[8] S.L. Topalian, F.S. Hodi, J.R. Brahmer, S.N. Gettinger, D.C. Smith, D.F. McDermott, J.D. Powderly, R.D. Carvajal, J.A. Sosman, M.B. Atkins, P.D. Leming, D.R. Spigel, S.J. Antonia, L. Horn, C.G. Drake, D.M. Pardoll, L. Chen, W.H. Sharfman, R.A. Anders, J.M. Taube, T.L. McMiller, H. Xu, A.J. Korman, M. Jure-Kunkel, S. Agrawal, D. McDonald, G.D. Kollia, A. Gupta, J.M. Wigginton, M. Sznol, Safety, activity, and immune correlates of anti-PD-1 antibody in cancer, N. Engl. J. Med. 366 (2012) 2443–2454.

[9] R. Maxwell, C.M. Jackson, M. Lim, Clinical trials investigating immune checkpoint blockade in glioblastoma, Curr. Treat. Options in Oncol. 18 (2017) 51.

[10] R.H. Thompson, S.M. Kuntz, B.C. Leibovich, H. Dong, C.M. Lohse, W.S. Webster, S. Sengupta, I. Frank, A.S. Parker, H. Zincke, M.L. Blute, T.J. Sebo, J.C. Cheville, E.D. Kwon, Tumor B7-H1 is associated with poor prognosis in renal cell carcinoma patients with long-term follow-up, Cancer Res. 66 (2006) 3381–3385.

[11] R. Hino, K. Kabashima, Y. Kato, H. Yagi, M. Nakamura, T. Honjo, T. Okazaki, Y. Tokura, Tumor cell expression of programmed cell death-1 ligand 1 is a prognostic factor for malignant melanoma, Cancer 116 (2010) 1757–1766.

[12] R.H. Thompson, M.D. Gillett, J.C. Cheville, C.M. Lohse, H. Dong, W.S. Webster, K.G. Krejci, J.R. Lobo, S. Sengupta, L. Chen, H. Zincke, M.L. Blute, S.E. Strome, B.C. Leibovich, E.D. Kwon, Costimulatory B7-H1 in renal cell carcinoma patients: indicator of tumor aggressiveness and potential therapeutic target, Proc. Natl. Acad. Sci. U. S. A. 101 (2004) 17174–17179.

[13] J. Hamanishi, M. Mandai, M. Iwasaki, T. Okazaki, Y. Tanaka, K. Yamaguchi, T. Higuchi, H. Yagi, K. Takakura, N. Minato, T. Honjo, S. Fujii, Programmed cell death 1 ligand 1 and tumor-infiltrating CD8+ T lymphocytes are prognostic factors of human ovarian cancer, Proc. Natl. Acad. Sci. U. S. A. 104 (2007) 3360–3365.

[14] H. Ghebeh, A. Tulbah, S. Mohammed, N. Elkum, S.M. Bin Amer, T. Al-Tweigeri, S. Dermime, Expression of B7-H1 in breast cancer patients is strongly associated with high proliferative Ki-67-expressing tumor cells, Int. J. Cancer 121 (2007) 751–758.

[15] J. Chen, C.C. Jiang, L. Jin, X.D. Zhang, Regulation of PD-L1: a novel role of pro-survival signalling in cancer, Ann. Oncol. 27 (2016) 409–416.

[16] X. Zhang, Y. Zeng, Q. Qu, J. Zhu, Z. Liu, W. Ning, H. Zeng, N. Zhang, W. Du, C. Chen, J.A. Huang, PD-L1 induced by IFN-gamma from tumor-associated macrophages via the JAK/STAT3 and PI3K/AKT signaling pathways promoted progression of lung cancer, Int. J. Clin. Oncol. 22 (2017) 1026–1033.

[17] C.A. Clark, H.B. Gupta, G. Sareddy, S. Pandeswara, S. Lao, B. Yuan, J.M. Drerup, A. Padron, J. Conejo-Garcia, K. Murthy, Y. Liu, M.J. Turk, K. Thedieck, V. Hurez, R. Li, R. Vadlamudi, T.J. Curiel, Tumor-intrinsic PD-L1 signals regulate cell growth, pathogenesis, and autophagy in ovarian cancer and melanoma, Cancer Res. 76 (2016) 6964–6974.

[18] J. Li, L. Chen, Y. Xiong, X. Zheng, Q. Xie, Q. Zhou, L. Shi, C. Wu, J. Jiang, H. Wang, Knockdown of PD-L1 in human gastric cancer cells inhibits tumor progression and improves the cytotoxic sensitivity to CIK therapy, Cell. Physiol. Biochem. 41 (2017) 907–920.

[19] L. Zhao, C. Li, F. Liu, Y. Zhao, J. Liu, Y. Hua, J. Liu, J. Huang, C. Ge, A blockade of PD-L1 produced antitumor and antimetastatic effects in an orthotopic mouse pancreatic cancer model via the PI3K/Akt/mTOR signaling pathway, Onco Targets Ther. 10 (2017) 2115–2126.

[20] C.Y. Ock, S. Kim, B. Keam, M. Kim, T.M. Kim, J.H. Kim, Y.K. Jeon, J.S. Lee, S.K. Kwon, J.H. Hah, T.K. Kwon, D.W. Kim, H.G. Wu, M.W. Sung, D.S. Heo, PD-L1 expression is associated with epithelial-mesenchymal transition in head and neck squamous cell carcinoma, Oncotarget 7 (2016) 15901–15914.

[21] S. Kim, J. Koh, M.Y. Kim, D. Kwon, H. Go, Y.A. Kim, Y.K. Jeon, D.H. Chung, PD-L1 expression is associated with epithelial-to-mesenchymal transition in adenocarcinoma of the lung, Hum. Pathol. 58 (2016) 7–14.

[22] H.B. Gupta, C.A. Clark, B. Yuan, G. Sareddy, S. Pandeswara, A.S. Padron, V. Hurez, J. Conejo-Garcia, R. Vadlamudi, R. Li, T.J. Curiel, Tumor cell-intrinsic PD-L1 promotes tumor-initiating cell generation and functions in melanoma and ovarian cancer, Signal Transduct. Target. Ther. 1 (2016).

[23] S. Xue, G. Song, J. Yu, The prognostic significance of PD-L1 expression in patients with glioma: a meta-analysis, Sci. Rep. 7 (2017) 4231.

[24] Y. Yao, R. Tao, X. Wang, Y. Wang, Y. Mao, L.F. Zhou, B7-H1 is correlated with malignancy-grade gliomas but is not expressed exclusively on tumor stem-like cells, Neuro-Oncology 11 (2009) 757–766.

[25] Z. Wang, C. Zhang, X. Liu, Z. Wang, L. Sun, G. Li, J. Liang, H. Hu, Y. Liu, W. Zhang, T. Jiang, Molecular and clinical characterization of PD-L1 expression at transcriptional level via 976 samples of brain glioma, Oncoimmunology 5 (2016) e1196310.

[26] E.K. Nduom, J. Wei, N.K. Yaghi, N. Huang, L.Y. Kong, K. Gabrusiewicz, X. Ling, S. Zhou, C. Ivan, J.Q. Chen, J.K. Burks, G.N. Fuller, G.A. Calin, C.A. Conrad, C. Creasy, K. Ritthipichai, L. Radvanyi, A.B. Heimberger, PD-L1 expression and prognostic impact in glioblastoma, Neuro-Oncology 18 (2016) 195–205.

[27] J. Zeng, X.K. Zhang, H.D. Chen, Z.H. Zhong, Q.L. Wu, S.X. Lin, Expression of programmed cell death-ligand 1 and its correlation with clinical outcomes in gliomas, Oncotarget 7 (2016) 8944–8955.

[28] S. Xue, M. Hu, P. Li, J. Ma, L. Xie, F. Teng, Y. Zhu, B. Fan, D. Mu, J. Yu, Relationship between expression of PD-L1 and tumor angiogenesis, proliferation, and invasion in glioma, Oncotarget 8 (30) (2017) 49702–49712.

[29] J. Joung, S. Konermann, J.S. Gootenberg, O.O. Abudayyeh, R.J. Platt, M.D. Brigham, N.E. Sanjana, F. Zhang, Genome-scale CRISPR-Cas9 knockout and transcriptional activation screening, Nat. Protoc. 12 (2017) 828–863.

[30] N.E. Sanjana, O. Shalem, F. Zhang, Improved vectors and genome-wide libraries for CRISPR screening, Nat. Methods 11 (2014) 783–784.

[31] C. Depner, H. Zum Buttel, N. Bogurcu, A.M. Cuesta, M.R. Aburto, S. Seidel, F. Finkelmeier, F. Foss, J. Hofmann, K. Kaulich, S. Barbus, M. Segarra, G. Reifenberger, B.K. Garvalov, T. Acker, A. Acker-Palmer, EphrinB2 repression through ZEB2 mediates tumour invasion and anti-angiogenic resistance, Nat. Commun. 7 (2016) 12329.

[32] J.M. Drake, C.L. Gabriel, M.D. Henry, Assessing tumor growth and distribution in a model of prostate cancer metastasis using bioluminescence imaging, Clin. Exp. Metastasis 22 (2005) 674–684.

[33] J. Zhang, S.J. Lan, Q.R. Liu, J.M. Liu, X.Q. Chen, Neuroglobin, a novel intracellular hexa-coordinated globin, functions as a tumor suppressor in hepatocellular carcinoma via Raf/MAPK/Erk, Mol. Pharmacol. 83 (2013) 1109–1119.

[34] Y. Chen, J.M. Liu, X.X. Xiong, X.Y. Qiu, F. Pan, D. Liu, S.J. Lan, S. Jin, S.B. Yu, X.Q. Chen, Piperlongumine selectively kills hepatocellular carcinoma cells and preferentially inhibits their invasion via ROS-ER-MAPKs-CHOP, Oncotarget 6 (2015) 6406–6421.

[35] Y. Lu, L. Xiao, Y. Liu, H. Wang, H. Li, Q. Zhou, J. Pan, B. Lei, A. Huang, S. Qi, MIR517C inhibits autophagy and the epithelial-to-mesenchymal (−like) transition phenotype in human glioblastoma through KPNA2-dependent disruption of TP53 nuclear translocation, Autophagy 11 (2015) 2213–2232.

[36] L. Li, Q.R. Liu, X.X. Xiong, J.M. Liu, X.J. Lai, C. Cheng, F. Pan, Y. Chen, S.B. Yu, A.C. Yu, X.Q. Chen, Neuroglobin promotes neurite outgrowth via differential binding to PTEN and Akt, Mol. Neurobiol. 49 (2014) 149–162.

[37] S. Lamouille, J. Xu, R. Derynck, Molecular mechanisms of epithelial-mesenchymal transition, Nat. Rev. Mol. Cell Biol. 15 (2014) 178–196.

[38] R. Virtakoivu, A. Mai, E. Mattila, N. De Franceschi, S.Y. Imanishi, G. Corthals, R. Kaukonen, M. Saari, F. Cheng, E. Torvaldson, V.M. Kosma, A. Mannermaa, G. Muharram, C. Gilles, J. Eriksson, Y. Soini, J.B. Lorens, J. Ivaska, Vimentin-ERK signaling uncouples slug gene regulatory function, Cancer Res. 75 (2015) 2349–2362.

[39] J.A. McCubrey, T.L. Fitzgerald, L.V. Yang, K. Lertpiriyapong, L.S. Steelman, S.L. Abrams, G. Montalto, M. Cervello, L.M. Neri, L. Cocco, A.M. Martelli, P. Laidler, J. Dulinska-Litewka, D. Rakus, A. Gizak, F. Nicoletti, L. Falzone, S. Candido, M. Libra, Roles of GSK-3 and microRNAs on epithelial mesenchymal transition and cancer stem cells, Oncotarget 8 (2017) 14221–14250.

[40] A. Takashima, D.V. Faller, Targeting the RAS oncogene, Expert Opin. Ther. Targets 17 (2013) 507–531.

[41] M.K. Callahan, M.A. Postow, J.D. Wolchok, Targeting T cell co-receptors for cancer therapy, Immunity 44 (2016) 1069–1078.

[42] A.S. Berghoff, B. Kiesel, G. Widhalm, O. Rajky, G. Ricken, A. Wohrer, K. Dieckmann, M. Filipits, A. Brandstetter, M. Weller, S. Kurscheid, M.E. Hegi, C.C. Zielinski, C. Marosi, J.A. Hainfellner, M. Preusser, W. Wick, Programmed death ligand 1 expression and tumor-infiltrating lymphocytes in glioblastoma, Neuro-Oncology 17 (2015) 1064–1075.

[43] U.D. Kahlert, D. Maciaczyk, S. Doostkam, B.A. Orr, B. Simons, T. Bogiel, T. Reithmeier, M. Prinz, J. Schubert, G. Niedermann, T. Brabletz, C.G. Eberhart, G. Nikkhah, J. Maciaczyk, Activation of canonical WNT/beta-catenin signaling enhances in vitro motility of glioblastoma cells by activation of ZEB1 and other

activators of epithelial-to-mesenchymal transition, Cancer Lett. 325 (2012) 42–53.
[44] H.A. Kim, B.K. Koo, J.H. Cho, Y.Y. Kim, J. Seong, H.J. Chang, Y.M. Oh, D.E. Stange, J.G. Park, D. Hwang, Y.Y. Kong, Notch1 counteracts WNT/beta-catenin signaling through chromatin modification in colorectal cancer, J. Clin. Invest. 122 (2012) 3248–3259.
[45] N. Cancer Genome Atlas Research, Comprehensive genomic characterization defines human glioblastoma genes and core pathways, Nature 455 (2008) 1061–1068.
[46] D.A. Nathanson, B. Gini, J. Mottahedeh, K. Visnyei, T. Koga, G. Gomez, A. Eskin, K. Hwang, J. Wang, K. Masui, A. Paucar, H. Yang, M. Ohashi, S. Zhu, J. Wykosky, R. Reed, S.F. Nelson, T.F. Cloughesy, C.D. James, P.N. Rao, H.I. Kornblum, J.R. Heath, W.K. Cavenee, F.B. Furnari, P.S. Mischel, Targeted therapy resistance mediated by dynamic regulation of extrachromosomal mutant EGFR DNA, Science (New York, N.Y.) 343 (2014) 72–76.